Dalton Transactions

Accepted Manuscript

This is an *Accepted Manuscript*, which has been through the Royal Society of Chemistry peer review process and has been accepted for publication.

Accepted Manuscripts are published online shortly after acceptance, before technical editing, formatting and proof reading. Using this free service, authors can make their results available to the community, in citable form, before we publish the edited article. We will replace this *Accepted Manuscript* with the edited and formatted *Advance Article* as soon as it is available.

You can find more information about *Accepted Manuscripts* in the Information for Authors.

ROYAL SOCIETY OF CHEMISTRY

www.rsc.org/dalton

Graphical abstract

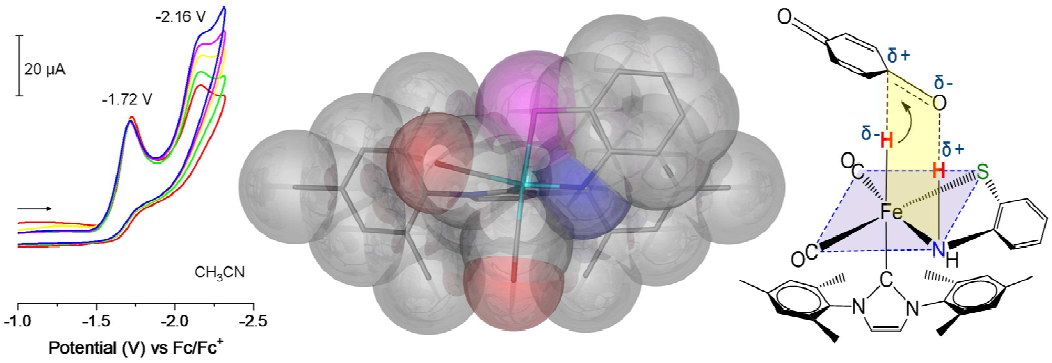

A novel pentacoordinate mono-iron dicarbonyl was reported as structural and functional model of [Fe]-hydrogenase active site.

Dalton Transactions

COMMUNICATION

Nitrogen Heterocyclic Carbene Containing Pentacoordinate Iron Dicarbonyl as [Fe]-hydrogenase Active Site Model†

Received 00th January 20xx,
Accepted 00th January 20xx

DOI: 10.1039/x0xx00000x

www.rsc.org/

Shuang Jiang,[a,b] Tianyong Zhang,[a,b,*] Xia Zhang,[a,b] Guanghui Zhang[a,b] and Bin Li[a,b,c,*]

A novel pentacoordinate mono iron dicarbonyl complex bearing a nitrogen heterocyclic carbene ligand was reported as model of [Fe]-hydrogenase active site, which exhibits interesting proton coupled CO bonding reactivity, electro-catalytic proton reduction and catalytic transfer hydrogenation reactivity.

Nature has evoked hydrogenase as an expert for efficient proton reduction and hydrogen oxidation which utilizes abundant first-row metals (Fe and Ni).[1] Typical hydrogenases include [FeFe]-hydrogenase and [NiFe]-hydrogenase that catalyze reversible proton reduction and hydrogen oxidation (H_2=$2H^+ + 2e^-$)[2] and [Fe]-hydrogenase which catalyzes the reversible reduction of N^5,N^{10}-methenyl-tetrahydromethanopterin (MPT^+) with H_2 to N^5,N^{10}-methylene-tetrahydromethanopterin (HMPT) and a proton **(Figure 1(a))**.[3] Recent study of the [Fe]-hydrogenase active site revealed that a mono iron center has a pseudo-octahedral coordination with a cysteine sulfur atom, two *cis*-CO ligands, a bidentate pyridone ligand through its nitrogen and acyl carbon atoms, and an open site (or a H_2O) *trans* to the acyl group **(Figure 1(a))**.[4] Some synthetic structural analogues of [Fe]-hydrogenase have been developed that mimic first coordination sphere of the iron in [Fe]-hydrogenase.[5,6] However, due to the lack of suitable substrate, cofactors, similar geometric and electronic environment, it is still being a great challenge to develop functional analogues of the [Fe]-hydrogenase active site.

Recently, hydrogen activation and transfer by first-row transition metals especially Fe and Ni have received increased interest due to the high abundance, low price and low toxicity of the metals. Abundant functional [FeFe]-hydrogenase and [NiFe]-hydrogenase analogues were developed.[7-10] However, only the biological and theoretical investigation have been conducted for the function of [Fe]-hydrogenase.[11] The ternary-complex mechanism does not invoke an Fe-H intermediary, **Figure 1(a)**. While DFT calculations suggest that hydrogen activation proceeds following the formation of a dihydrogen, Fe-$H^{\delta-}$…$H^{\delta+}$-O, bond and substrate (MPT^+) triggered hydride transfer mechanism, **Figure 1(b)**. It is notable that the key transition state in this calculated mechanism actually bears a six membered ring of -Fe-H-H-O-C-N-.

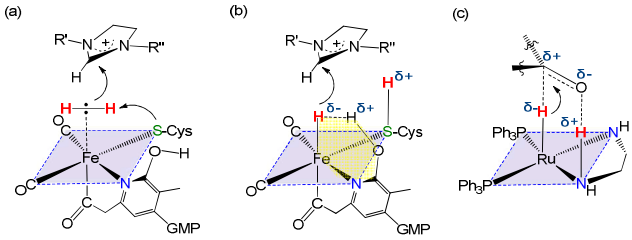

Figure 1. (a) Structure of the active-site of the [Fe]-hydrogenase and suggested mechanism (non-hydride); (b) DFT calculated hydride transfer mechanism for [Fe]-hydrogenase catalytic process; (c) H_2 activation and catalytic hydrogenation of ketone by Ru complex via a six-member ring transition state.

The asymmetric hydrogenation of ketones by the phosphine/diamine Ru complexes via a non–classical metal-ligand bifunctional catalysis mechanism has been well established **(Figure 1(c))**.[12] Recently, similar iron complexes were also developed for the catalytic reduction of C=O or C=N.[13] The ancillary ligand with NH group played a crucial role in the hydride transfer. Aiming at developing a potential functional model of [Fe]-hydrogenase, we aimed to synthesize a pentacoordinate mono iron analogue that concurrently exhibited both the similar first coordination sphere and the never-reported catalytic reduction functions. In this communication, we report the synthesis, structural characterization and the coordination reactivity of a [Fe]-hydrogenase model, which serves as a bifunctional catalyst for catalytic proton reduction and transfer hydrogenation.

Synthesis of complex **1** follows the procedure outlined in **Figure 2(a)**. Due to the excellent electron donor ability of the nitrogen heterocyclic carbene ligand, complex **1** was isolated successfully as

[a] *School of Chemical Engineering and Technology, Tianjin Key Laboratory of Applied Catalysis Science and Technology, Tianjin University, Tianjin 300072, China.*
[b] *Collaborative Innovation Center of Chemical Science and Engineering (Tianjin), Tianjin 300072, China.*
[c] *State Key Laboratory of Fine Chemicals, Dalian University of Technology, Dalian 116024, China*

†Electronic Supplementary Information (ESI) available: Experimental procedures, additional spectroscopic details, electrochemistry, X-ray crystallographic data (CIF) obtained from the structure determination and a full list of metric parameters for complexes **1**. CCDC 1040792. For ESI and crystallographic data in CIF or other electronic format see DOI: 10.1039/c000000x/

an air stable dark crystalline solid in good yield. Unlike similar phosphine and cyanide derived complexes,[14] the target complex **1** is rather stable and could be handled in air and stored at room temperature for months. Furthermore, the solution form of **1** in methanol (or ethanol) is relatively thermal (50°C) and light stable, which enables its potential application in catalytic hydrogenation reactions. **Figure S1** displays the ***ν***(CO) IR spectra (measured in CH_2Cl_2, 1987 and 1927cm^{-1}) of **1** for which the near equal intensity of the two bands suggests that *cis*-dicarbonyls are about 90° angles as those of the [Fe]-hydrogenase active site.[4]

The single crystals suitable for X-ray diffraction study were grown by slow evaporation of a diethyl ether solution of complex **1** at room temperature. The molecular structure is presented in **Figure 2(b)** to emphasize the square pyramidal structure of complex **1** for which analysis according to Addison's τ value[15] finds complex **1** (τ = 0.506, based on α(C1Fe1S1)= 172.12 and β(C2Fe1N3) = 141.77) to be approximated as a square pyramid. The two CO ligands and the IMes ligand reflect their *trans* influence. The nitrogen and sulfur ligand is *cis* to the IMes ligand and the position *trans* to the latter is vacant. The C1-Fe1-C2 angle of 91.78(6)° coincided with the IR spectrum of two *cis*-CO ligands. The Fe-C3(IMes) bond of 1.9535(12)Å in **1** is shorter than that of 2.002(6)Å in the precursor of $FeI_2(CO)_3$IMes[6], which is consistent with the good stability of **1**, and fits well with the other reported Fe-NHC complexes.[16] The selected metric data, bond length and angles are listed in **Table S2-S3.** The 2-amidothiophenolate dianion bidentate ligand is parallel to the mesityl group flanking the carbene donor, **Figure S11**.

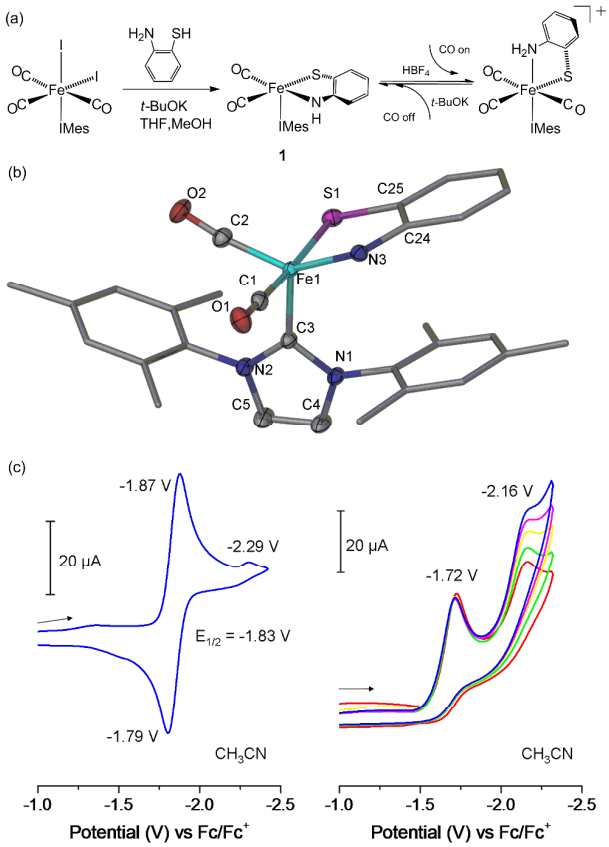

Figure 2. (a) synthetic route and proton coupled CO bonding activity of complex **1**, (b) X-ray crystal structure of complex **1**, hydrogen atoms are omitted for clarity. (c) Left: cyclic voltammograms of complex **1** (2.5 mM), Right: CV of complex **1** with added AcOH (5, 7.5, 10, 12.5, and 15mM) in CH_3CN solution, scan rate = 50mV.

The reactivity with CO was examined due to the unsaturated coordination sphere of complex **1** as well as to mimic the [Fe]-hydrogenase active site which readily binded CO to yield a facial tricarbonyl species. Complex **1** showed no reactivity with CO under room temperature and atmospheric pressure. Moreover **1** will decomposed in minutes after the addition of strong acid HBF_4 under N_2 atomsphere. Nevertheless, a proton coupled CO binding reactivity is observed, **Figure 2(a)**. In the presence of HBF_4 and CO (0.1MPa), solution of complex **1** in ethanol undergo a color change from dark brown to orange with concomitant ν(CO) spectral changes indicating that *mer*-$[Fe(CO)_3IMes(H\text{-}NS)]^+$ (2102(w), 2053 (s) and 2031 (m) cm^{-1} in ethanol solution (**Figure S2**), formed via stoichiometric CO binding. On deprotonation with *t*-BuOK or Et_3N, CO is released and complex **1** is regenerated, **Figure S2**.

The electrochemistry of complex **1** was studied by cyclic voltammetry (CV) in CH_3CN in the presence of Bu_4NPF_6 as supporting electrolyte with the goal of evaluating its redox properties. Complex **1** exhibits a reversible reductive event at $E_{1/2}$= -1.83V vs $Fc^{+/0}$, which is attributed to the couple Fe^{II}/Fe^{I} (**Figure 2(c)**) according to relative [FeFe]-hydrogenase models.[17] The second reduction event at -2.29V was assigned to the couple Fe^{I}/Fe^{0}, which was not observed under the higher scan rate of 200mV/s, **Figure S8**. Upon addition of AcOH (2eq.) to the CH_3CN solution of complex **1**, the first reduction peak showed an anodic shift by 150mV and the current intensity did not increase with the incremental addition of the acid. The second reduction peak at -2.29V resulted in a positive shift by 130mV. The current of the second reduction peak observed at -2.16V increased linearly with increasing acid (AcOH) concentration (2, 3, 4, 5, and 6eq.), **Figure S5**, which is attributed to catalytic proton reduction. It is notable that the reduction peak moved to more positive potentials in the presence of AcOH, consistent with the protonation of amine group as in other diiron hydrogenase models, **Figure S4**.[18] Based on such series of events, a CEEC (Chemical-Electrochemical-Electrochemical-Chemical) mechanism was probably involved in this catalytic hydrogen production, **Figure S7**. In the presence of AcOH, complex **1** is protonated on the ligand-N atom to form $[(Fe^{II})(NH_2)]^+$ ($[(1(H)]^+$), which undergoes a two-step reduction to form $[(Fe^{I})(NH_2)]$ ([1(H)]) and $[(Fe^{0})(NH_2)]^-$ ($[(1(H)]^-$) in a stepwise manner. The further protonation of electron-enriched $[1(H)]^-$ generate a $[(HFe^{II})(NH_2)]$ ([1(H-H)]) intermediate, which can evolve to H_2 to fullfill the catalytic cycle.

The adjustment of electronic properties of the iron center by protonation of the ligand-N atom leads us to examine the possible catalytic hydrogenation reactivity of this complex. Inspired by the Coenzyme Q and vitamin K_2 in nature, which have the quinone or hydroquinone sections in their structures, 1,4-benzoquinone comes into our sight.[19] Quinone-hydroquinone couple is a typical organic redox case and the research on the electrochemical behavior of this couple has drawn scientists' attention for nearly one century. The reported reduction of 1,4-benzoquinone were usually achieved by typical chemical reductant or catalytic hydrogenation based on Ni,

Pd or Pt catalyst.[20] Since quinones play key roles in living bodies, many investigations have been made about the redox behavior of quinone-hydroquinone[21] From the electron transfer chain (ETC) in the case of coupled electron transfer to the movement of protons, H_2 could acts as an inorganic electron donor and quinone as carriers.[22] Therefore we used complex **1** to activate H_2 under mild conditions with the assistance of 1,4-benzoquinone in methanol, from which we found that 1,4-benzoquinone was reduced to hydroquinone with a high conversion rate, which easily mislead us to assure that H_2 was activated. While the control experiment without a H_2 atomsphere revealed that a transfer hydrogenation process with methanol as the proton source rather than H_2 was probably involved here.[13]

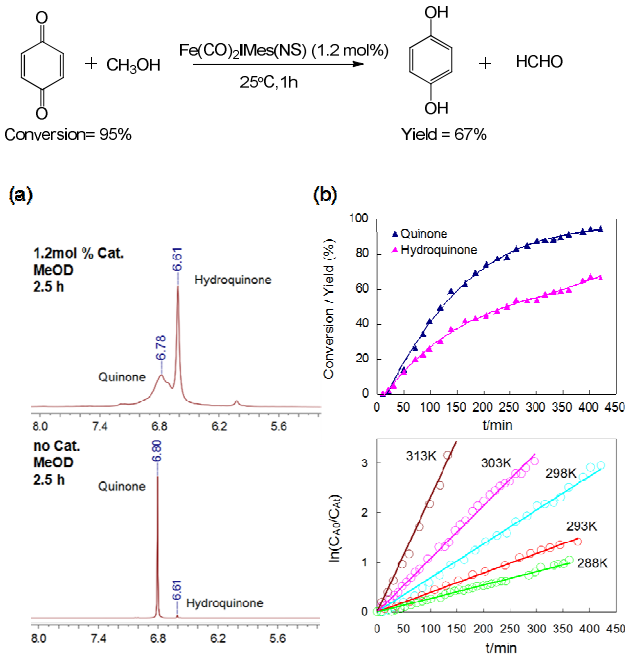

Figure 3. (a)Top: In-situ ^{1}H NMR monitor of the catalytic transfer hydrogenation reaction of quinone at 25°C in 0.5 h. Bottom: Control experiment under the similar conditions without addition of complex 1; (b) Top: Dependence of conversion of quinone and yield of hydroquinone on time at 25°C, 1.2 mol% complex 1. Bottom: Natural log plots of concentration of quinone verse time at various temperatures, 1.2mol% complex 1.

In-situ ^{1}H NMR study was utilized to examine such a transfer hydrogenation process. Quinone and 1.2mol% complex **1** was dissolved in MeOD and it was observed that about 60% of 1,4-benzoquinone (chemical shift 6.78ppm) transformed to hydroquinone (chemical shift 6.61ppm) in 2.5h, **Figure 3(a)**. In contrast, the control experiment without **1** as catalyst showed no obvious change in the concentration of quinone under the same conditions, **Figure 3(a)**. The slight peak of hydroquinone at 6.61ppm was attributed to the impurity of standard commercial quinone reagent with comparison, **Figure S12(b)**.

Furthermore, the transfer hydrogenation reaction of quinone catalyzed by 1.2mol% complex **1** in methanol at room temperature gave conversion of quinone over 95% and yield of hydroquinone ca. 67% in 7h, **Figure 3(b)**. The dependency of quinone concentration verses time fits well with an exponential function, **Figure S18**. In contrast, quinone was not reduced under the similar reaction conditions when no catalyst of complex **1** was adopted, **Figure S21**. **Table 1** shows the transfer hydrogenation of quinone with different H donors. It is illustrated that the reaction in ethanol proceeds a bit slower than in methanol and the reaction in isopropanol needs sufficient time to achieve a low conversion of 20% of quinone. It is notable that the tertiary butanol could not serve as proton source at all.

To further elucidate the mechanism of this transfer hydrogenation of quinone, kinetic studies were conducted. The reactions were carried out under pseudo-first-order conditions of excess methanol at a fixed molar ratio of catalyst (1.2 mmol% Cat.). Plots of $\ln(C_{A0}/C_{At})$ verses time showed good linearity, **Figure 3(b)**, which demonstrates that the reaction of catalytic transfer hydrogenation is first order with respect to quinone concentration. The temperature dependence of observed rate constants for transfer hydrogenation of quinone are given in **Table S4** and presented graphically as Arrhenius and Eyring plots, **Figure S22**. The small values of *E*a (64.3kJ/mol) and $\Delta H^{\ddagger}$ (61.8kJ/mol) as well as large negative value for $\Delta S^{\ddagger}$ (-113.1 J/mol K) are consistent with an associative pathway.

Table 1 Transfer hydrogenation of quinone with different H donors

Entry	H donor	Reaction time (h)	Conversion of Q (%)	Yield of HQ (%)
1	MeOH	7	95	67
2	EtOH	7	91	63
3	*i*-PrOH	7	14	5
4	*i*-PrOH	14	20	12
5	*t*-BuOH	14	0	0

Q = quinone; HQ = hydroquinone.

Scheme 1. Proposed pathway for catalytic transfer hydrogenation of quinone.

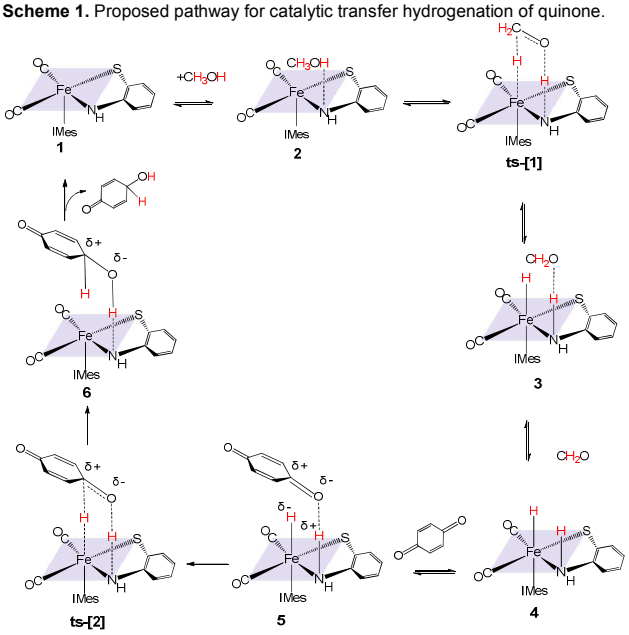

Taking into consideration of our current findings and previous studies,[13,23] we propose a mechanism of transfer hydrogenation

shown in **Scheme 1**. The amine-methanol specie **2** is first generated from complex **1** and methanol. Polarization of methanol by the iron center and amine ancillary would generate a transition state species **ts-[1]**, then the C-H and O-H bonds were fractured respectively, with a drop of methanol. With quinone conjuct to the proton and hydride simultaneously, a six-membered ring of -Fe-H-C-O-H-N- formed in **ts-[2]**. The dipole of quinone and easy formation of O-H-N hydrogen bond should respond to this transformation.[23] Then the hydride transfer from iron center to quinone carbon and the H-N bond split, generating hydroquinone finally. The species **ts-[2]** is similar to the DFT calculated [Fe]-hydrogenase catalytic process transition state demonstrated by Hall,[11] and coincided with the metal-ligand bifunctional catalytic system.[13,23]

Conclusions

In summary, we have provided a nitrogen heterocyclic carbene containing model of [Fe]-hydrogenase active site. Complex **1** not only reproduced the first coordination sphere, but also exhibited proton coupled CO bonding reactivity with the unsaturated coordinate open site. Moreover this complex catalyzed electrochemical catalytic proton reduction and quinone redcution via cleavage of CH_3OH by the iron center and build-in amine ligand. The hydrogen transfer via this molecular catalyst platform also provides insight into the function of [Fe]-hydrogenase. Based on insights obtained regarding the effect of amine auxiliary and C=O dipole substrate, the design and development of mono-iron catalysts with more efficient activity and better substrate adaptability are ongoing in our laboratory.

Notes and references

1 J. C. Fontecilla-Camps, A. Volbeda, C. Cavazza and Y. Nicolet, *Chem Rev*, 2007, **107**, 4273; L. Sun, B. Aakermark and S. Ott, *Coordin Chem Rev*, 2005, **249**, 1653; F. A. Armstrong and J. C. Fontecilla-Camps, *Science*, 2008, **321**, 498; F. Gloaguen and T. B. Rauchfuss, *Chem Soc Rev*, 2009, **38**, 100; C. Tard and C. J. Pickett, *Chem Rev*, 2009, **109**, 2245; K. M. Schultz, D. Chen and X. Hu, *Chem Asian J*, 2013, **8**, 1068; I. P. Georgakaki, L. M. Thomson, E. J. Lyon, M. B. Hall and M. Y. Darensbourg, *Coordin Chem Rev*, 2003, **238-239**, 255; W. Lubitz, H. Ogata, O. Rüdiger and E. Reijerse, *Chem Rev*, 2014, **114**, 4081.

2 J. W. Peters, W. N. Lanzilotta, B. J. Lemon and L. C. Seefeldt, *Science*, 1998, **282**, 1853; M. L. Helm, M. P. Stewart, R. M. Bullock, M. R. DuBois and D. L. DuBois, *Science*, 2011, **333**, 863; S. Ogo, K. Ichikawa, T. Kishima, T. Matsumoto, H. Nakai, K. Kusaka and T. Ohhara, *Science*, 2013, **339**, 682; K. Weber, T. Krämer, H. S. Shafaat, T. Weyhermüller, E. Bill, M. van Gastel, F. Neese and W. Lubitz, *J Am Chem Soc*, 2012, **134**, 20745.

3 T. Hiromoto, K. Ataka, O. Pilak, S. Vogt, M. S. Stagni, W. Meyer-Klaucke, E. Warkentin, R. K. Thauer, S. Shima and U. Ermler, *Febs Lett*, 2009, **583**, 585; S. Shima and R. K. Thauer, *Chem Rec*, 2007, **7**, 37; S. Vogt, E. J. Lyon, S. Shima and R. K. Thauer, *J Biol Inorg Chem*, 2008, **13**, 97; S. Dey, P. K. Das and A. Dey, *Coordin Chem Rev*, 2013, **257**, 42.

4 S. Shima, O. Pilak, S. Vogt, M. Schick, M. S. Stagni, W. Meyer-Klaucke, E. Warkentin, R. K. Thauer and U. Ermler, *Science*, 2008, **321**, 572.

5 D. F. Chen, R. Scopelliti and X. L. Hu, *J Am Chem Soc*, 2010, **132**, 928; D. F. Chen, R. Scopelliti and X. L. Hu, *Angew Chem Int Ed*, 2010, **49**, 7512; D. F. Chen, R. Scopelliti and X. L. Hu, *Angew Chem Int Ed*, 2011, **50**, 5671; A. M. Royer, M. Salomone-Stagni, T. B. Rauchfuss and W. Meyer-Klaucke, *J Am Chem Soc*, 2010, **132**, 16997; S. Tanino, Y. Ohki and K. Tatsumi, *Chem Asian J*, 2010, **5**, 1962; X. F. Wang, Z. M. Li, X. R. Zeng, Q. Y. Luo, D. J. Evans, C. J. Pickett and X. M. Liu, *Chem Commun*, 2008, 3555; L. C. Song, G. Y. Zhao, Z. J. Xie and J. W. Zhang, *Organometallics*, 2013, **32**, 2509; L. C. Song, F. Q. Hu, M. M. Wang, Z. J. Xie, K. K. Xu and H. B. Song, *Dalton Trans*, 2014, **43**, 8062.

6 B. Li, T. Liu, C. V. Popescu, A. Bilko and M. Y. Darensbourg, *Inorg Chem*, 2009, **48**, 11283; T. B. Liu, B. Li, C. V. Popescu, A. Bilko, L. M. Perez, M. B. Hall and M. Y. Darensbourg, *Chem-Eur J*, 2010, **16**, 3083.

7 R. P. Happe, W. Roseboom, A. J. Pierik, S. P. J. Albracht and K. A. Bagley, *Nature*, 1997, **385**, 126.

8 T. Liu, S. Chen, M. J. O'Hagan, M. Rakowski DuBois, R. M. Bullock and D. L. DuBois, *J Am Chem Soc*, 2012, **134**, 6257; T. Liu, D. L. DuBois and R. M. Bullock, *Nat Chem*, 2013, **5**, 228.

9 J. M. Camara and T. B. Rauchfuss, *J Am Chem Soc*, 2011, **133**, 8098; J. M. Camara and T. B. Rauchfuss, *Nature Chem*, 2012, **4**, 26.

10 N. Wang, M. Wang, Y. Wang, D. Zheng, H. Han, M. S. G. Ahlquist and L. Sun, *J Am Chem Soc*, 2013, **135**, 13688.

11 X. Yang and M. B. Hall, *J Am Chem Soc*, 2009, **131**, 10901; A. Dey, *J Am Chem Soc*, 2010, **132**, 13892; A. R. Finkelmann, M. T. Stiebritz and M. Reiher, *J Phys Chem B*, 2013, **117**, 4806.

12 M. Yamakawa, H. Ito and R. Noyori, *J Am Chem Soc*,, 2000, **122**, 1466.

13 W. Zuo, A. J. Lough, Y. F. Li and R. H. Morris, *Science*, 2013, **342**, 1080; D. S. Mérel, M. Elie, J.-F. Lohier, S. Gaillard and J.-L. Renaud, *ChemCatChem,*2013, **5**, 2939; A. vonderHöh and A. Berkessel, *ChemCatChem,* 2011, **3**, 861; C. P. Casey and H. R. Guan, *J Am Chem Soc,* 2007, **129**, 5816..

14 W. F. Liaw, N. H. Lee, C. H. Chen, C. M. Lee, G. H. Lee and S. M. Peng, *J Am Chem Soc*, 2000, **122**, 488.

15 A. W. Addison, T. N. Rao, J. Reedijk, J. van Rijn and G. C. Verschoor, *J Chem Soc, Dalton Trans*, 1984, 1349.

16 C.-H. Hsieh, R. Pulukkody and M. Y. Darensbourg, *Chem Commun*, 2013, **49**, 9326.

17 F. Gloaguen, J. D. Lawrence, M. Schmidt, S. R. Wilson and T. B. Rauchfuss, *J Am Chem Soc*, 2001, **123**, 12518; R. Mejia-Rodriguez, D. Chong, J. H. Reibenspies, M. P. Soriaga and M. Y. Darensbourg, *J Am Chem Soc*, 2004, **126**, 12004.

18 T. Liu, M. Wang, Z. Shi, H. Cui, W. Dong, J. Chen, B. Åkermark and L. Sun, *Chem-Eur J*, 2004, **10**, 4474.

19 S. Bhalerao and T. R. Clandinin, *Science*, 2012, **336**, 1241.

20 L. F. Fieser, *J Am Chem Soc*, 1928, **50**, 439; A. F. Barrero, E. J. Alvarez-Manzaneda, R. Chahboun and R. Meneses, *Synlett*, 1999, **10**, 1663; F. Algi and M. Balci, *Synth Commun*, 2006, **36**, 2293.

21 M. P. Soriaga and A. T. Hubbard, *J Am Chem Soc,* 1982, **104**, 273; S. Zhang, K. Wu and S. Hu, *Anal Chem*, 2002, **18**, 1089.

22 M. H. B. Stowell, T. M. McPhillips, D. C. Rees, S. M. Soltis, E. Abresch and G. Feher, *Science*, 1997, **276**, 812.

23 Ryoji Noyori, Masatoshi Koizumi, Dai Ishii and T. Ohkuma, *Pure Appl Chem*, 2001, **73**, 227.

Nitrogen Heterocyclic Carbene Containing Pentacoordinate Iron Dicarbonyl as [Fe]-hydrogenase Active Site Model

Shuang Jiang [a,b], Tianyong Zhang [a,b,*], Xia Zhang [a,b], Guanghui Zhang [a,b], and Bin Li [a,b,c,*]

[a] *Tianjin Key Laboratory of Applied Catalysis Science and Technology, School of Chemical Engineering and Technology, Tianjin University, Tianjin 300072, China*

[b] *Collaborative Innovation Center of Chemical Science and Engineering (Tianjin), Tianjin 300072, China*

[c] *State Key Laboratory of Fine Chemicals, Dalian University of Technology, Dalian 116024, China*

Experimental Section

Materials and Instruments

The synthetic reactions and operations were carried out on a double manifold Schlenk vacuum line under a N_2 atmosphere with rigorous exclusion of light. The solvents were dried and distilled prior to use according to the standard methods. The purified solvents were stored with molecular sieves under a nitrogen atmosphere for no more than 1 week before use. Complexes $FeI_2(CO)_4$ and $FeI_2(CO)_3$IMes were prepared according to the literature procedures.[1-2] The following materials were of reagent grade and available commercially from Sigma-Aldrich: 1,3-bis(2,4,6-trimethylphenyl) imidazolium chloride, potassium tert-butoxide, 2-aminothiophenol and nBu$_4$NPF$_6$. The $Fe(CO)_5$ was obtained freely from Jiangsu Tianyi Ultra-fine Metal Powder Co., Ltd (China).

The NMR spectra were measured on a Bruker AVANCE III 400MHz NMR spectrometer. ^{1}H and ^{13}C NMR shifts were referenced to residual solvent resonances according to the literature values. Solution IR spectra were recorded on a Shimadzu FTIR-8400 infrared spectrometer using 0.1mm KBr sealed cells. Quinone and hydroquinone samples were analyzed by a reversed phase high performance liquid

chromatography (C_{18}, Φ150×4.6mm) using the external standard method on an Agilent 1100 spectrometer. The mobile phase was CH_3CN/water (30/70, v/v), and the flow rate was 1.0mL/min. The measurement was performed at the wavelength of 298nm. Elemental analysis was carried out on a Heraeus CHN-Rapid, fully automatic elemental analyzer with TCD detection, type: TMT CHN, BESTELL-NR 2215001.

Synthetic Procedures.

$FeI_2(CO)_4$ and $FeI_2(CO)_3$IMes are both light and heat sensitive. Therefore, preparations, isolations, and manipulations were conducted in the dark. The isolated complex $Fe(CO)_2$IMes(NS) (**1**) was rather stable to light and heat (50°C), and could be handled in air as a solid and in the form of solution for more than 10h.

2 Equiv. of sodium tert-butoxide (112mg, 1.0mmol) in MeOH （10mL）was added dropwise to a MeOH (10ml) solution of 2-aminothiophenol (54μL, 0.5mmol) in a N_2 atmosphere, followed by vigorous stirring for an hour. The solvent was removed under vacuum and the residual dark solids were washed with diethyl ether (20mL). The residue was dried *in vacuo*, dissolved in methanol (10mL), then added into a THF (10mL) solution of $FeI_2(CO)_3$IMes (279mg, 0.4mmol) under a N_2 atmosphere. The reaction was monitored by IR to completion. The mixed solvent was removed *in vacuo* and the residual dark solids were extracted with diethyl ether (30mL). The ether was removed under vacuum to yield a dark red powder. Yield: 155mg (71.5%). The single crystals suitable for X-ray diffraction analysis were grown by slow evaporation of a diethyl ether solution of Complex **1** at -15°C. ^{1}H NMR (ppm, $CDCl_3$): δ = 8.99 (s, 1H, FeN<u>H</u>), 7.65(s, 1H, NC<u>H</u>), 6.97(s, 1H, NC<u>H</u>), 6.80(s, 4H, *m*-Mes), 2.27 (s, 6H, *p*-Mes), 2.01 (s, 12H, *o*-Mes). ^{13}C NMR (ppm, $CDCl_3$): δ = 216.48 (***C***O), 184.14, 163.96, 140.65, 139.33,

136.35, 135.62, 129.09, 128.07, 124.97, 121.80, 119.39, 118.62, 21.30, 18.05. IR (CH_2Cl_2, cm^{-1}): 1987 (s), 1927 (s). Elemental analysis, calc. for $C_{29}H_{29}O_2N_3SFe$: C, 64.56; H, 5.38; N, 7.79; S, 5.94. Found: C, 64.73; H,5.35; N, 7.78; S, 5.89.

CO Uptake of Complex 1 in the Presence of HBF_4

In a CO (0.1 MPa) atmosphere, complex **1** (15mg, 0.028mmol) dissolved in 10 mL ethanol was treated by the dropwise addition of HBF_4. The reaction was monitored by IR to indicate the generation of **[1(CO)-H]$^+$BF$_4^-$** (2102(w), 2053(s) and 2031(m) cm^{-1}) accompanied by a color change from dark brown to orange within 30 min. The treatment of **[1(CO)-H]$^+$BF$_4^-$** with *t*-BuOK led to the liberation of CO and stoichiometric regeneration of complex **1,** as monitored by IR. (see Figure S2)

X-ray Structure Determination of Complex $Fe(CO)_2$IMes(NS) (1)

The single-crystal of **1** was mounted on a Rigaku MM-007 diffractometer equipped with a Saturn 724CCD. Data were collected at 113K by using a confocal monochromator with Mo-Kα radiation (λ=0.71073 Å). Data collection, reduction and absorption correction were performed with the CRYSTALCLEAR program.[3] The structures were solved by direct methods using the SHELXS-97 program[4] and refined by the full-matrix least-squares techniques (SHELXL-97)[5] on F^2. Hydrogen atoms were located by geometrical calculation. Details of crystal data, data collections and structure refinements are summarized in Table S2 and Table S3.

Cyclic Voltammetry

Cyclic voltammograms were obtained in a three-electrode cell using a CHI 660B electrochemical workstation. A solution of 0.1 M nBu$_4$NPF$_6$ in CH_3CN was used as the supporting electrolyte. The electrolyte solution was degassed by bubbling dry N_2 through for 10 min before measurements. The working electrode was a glassy carbon disc with a diameter of 3 mm polished with 3 and 1 μm diamond pastes and sonicated in ion-free water for 20 min and washed by CH_3CN prior to use. The reference electrode was a non-aqueous Ag/Ag^+ (0.01M $AgNO_3$ in CH_3CN) electrode and the counter electrode was platinum wire. Ferrocene was used as an external standard under the same measuring conditions and all potentials are referenced to the $Cp_2Fe^{+/0}$ couple at 0 V. During the electrocatalytic experiments under N_2, increments of glacial HOAc (chromatographic grade,S99.8%, water 0.15%, by the Karl Fischer method) were added by microsyringe.

Kinetic Measurements

Pseudo-first-order reaction conditions were employed for all kinetic studies with 1.2 mol% catalyst of complex **1**. HPLC was used to monitor the concentration of quinone during the transfer hydrogenation reaction. In a typical experiment, 50 mg (0.46 mmol) quinone and 3 mg (0.0056 mmol) complex **1** was dissolved in 12.5 mL methanol. While being magnetically stirred, samples were taken at 8 to 40 min intervals typically through four reaction half-lives. Rates of the reactions were measured by following the decrease of concentration of quinone. Rate constants were calculated from plots of $\ln(A_0/A_t)$

versus time; activation parameters $\Delta H^{\ddagger}$, $\Delta S^{\ddagger}$ were obtained from Eyring plots; activation energies, E_a, were obtained from Arrhenius plots.

References

(1) B. Li, T. B. Liu, C. V. Popescu, A. Bilko, M. Y. Darensbourg, *Inorg Chem* **2009**, *48*, 11283.

(2) W. Hieber, G. Bader, *Ber. Dtsch. Chem. Ges.* **1928**, *61*, 1717.

(3) CRYSTALCLEAR 1.3.6. Rigaku and Rigaku/MSC (2005). 9009 New Trail Dr. The Woodlands TX 77381 USA.

(4) Sheldrick, G. M. SHELXS-97, A Program for Crystal Structure Solution; University of Göttingen: Germany, 1997.

(5) Sheldrick, G. M. SHELXL-97, A Program for Crystal Structure Refinement; University of Göttingen: Germany, 1997.

Table S1. Comparisons of *ν*(CO) absorption of $Fe(CO)_2IMes(NS)$ and some five coordinate Fe^{II} complexes derivatives (reported in CH_2Cl_2 solution unless otherwise noted; NS = aminothiophenylate).

Complexes	v(CO) (cm^{-1})	**Ref.**[a]
$Fe(CO)_2IMes(NS)$ **(1)**	1987(s), 1927(s)	this work
$Fe(CO)_2PCy_3(NS)$	1985(s), 1927(s)	(1)
$Fe(CO)_2PPh_3(NS)$	2002(s), 1942(s)	(1)
$Fe(CO)_2P(OEt)_3(NS)$	2012(s), 1956(s)	(1)
$[Fe(CO)_2(CN)(NS)]^-$	2000(s), 1936(s)	(2)
Hmd	2011(s), 1944(s)	(3)
Extracted cofactor	2031(s), 1972(s)	(3)
CO-inhibited Hmd	2074(s), 2020(s), 1981(s)	(3)
$[Fe(CO)_3IMes(NS)H^+]$	2102(w), 2053(s), 2031(m) (in EtOH)	this work
$[Fe(CO)_3PCy_3(NS)H^+]$	2102(w), 2046(vs)	(1)
$[FeI_2(CO)_3P(OEt)_3]$	2102(w), 2052(vs)	(1)

[a] **Ref.**:

(1) T. B. Liu, B. Li, C. V. Popescu, A. Bilko, L. M. Perez, M. B. Hall, M. Y. Darensbourg, *Chem-Eur J* **2010**, *16*, 3083.

(2) W. F. Liaw, N. H. Lee, C. H. Chen, C. M. Lee, G. H. Lee, S. M. Peng, *J Am Chem Soc* **2000**, *122*, 488.

(3) E. J. Lyon, S. Shima, R. Boecher, R. K. Thauer, F. W. Grevels, E. Bill, W. Roseboom, S. P. J. Albracht, *J Am Chem Soc* **2004**, *126*, 14239.

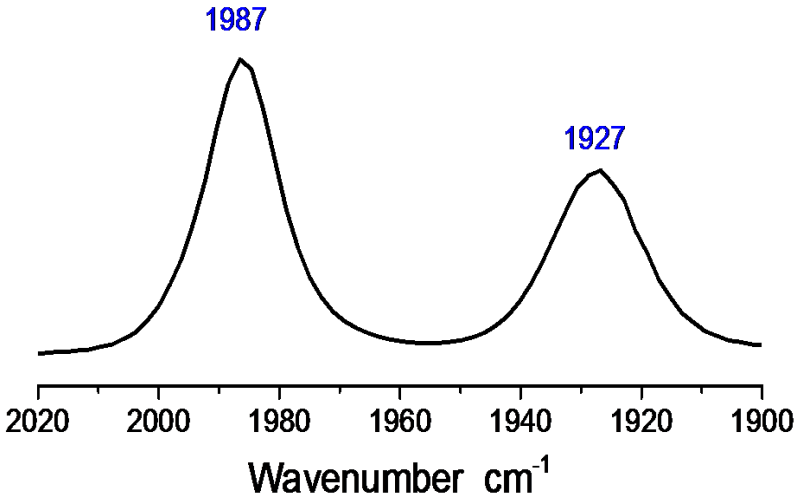

Figure S1. FT-IR spectrum of complex $Fe(CO)_2IMes(NS)$ recorded in CH_2Cl_2.

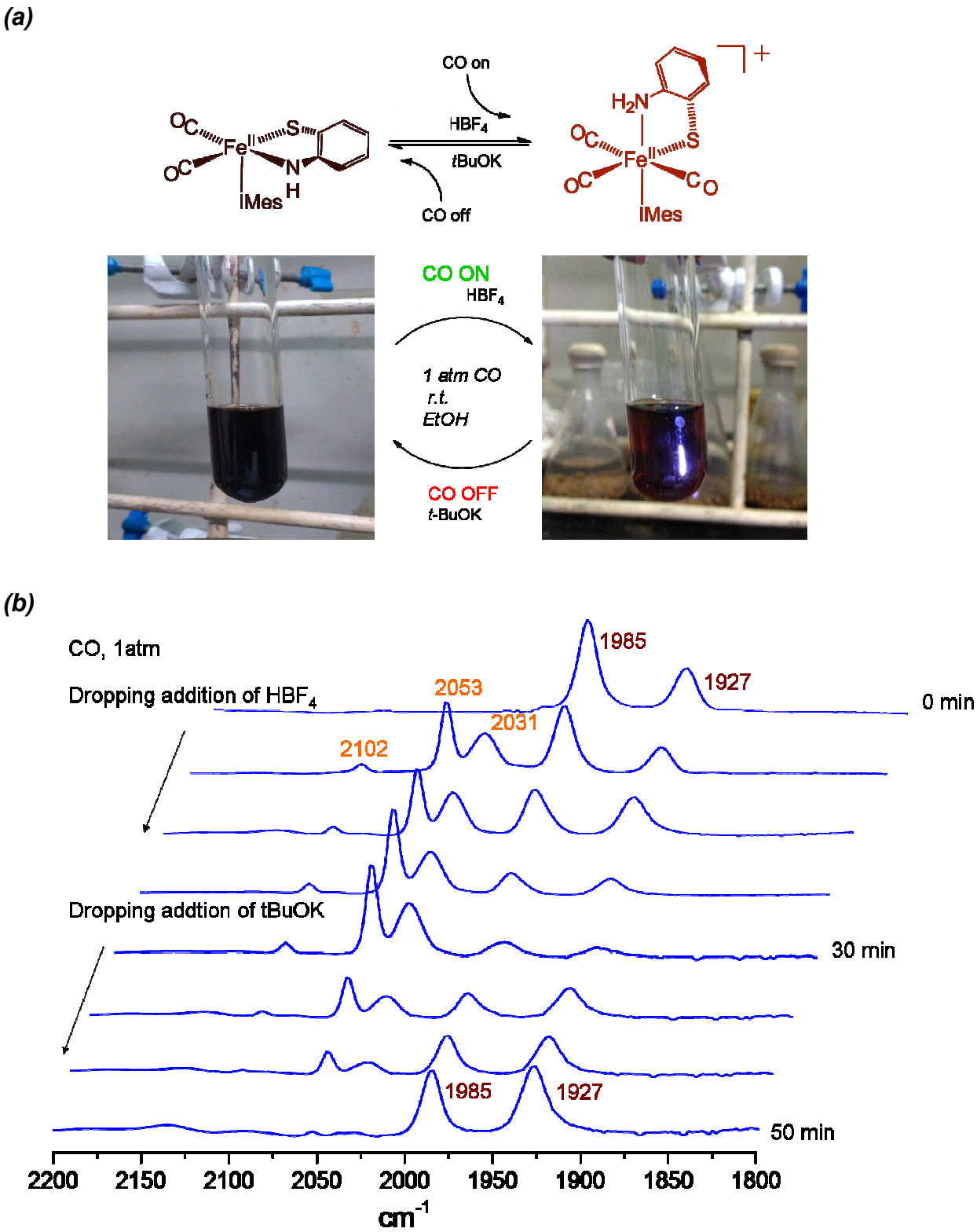

Figure S2. (a) Reversible CO uptake/release of complex **1** in the presence of acid/base. (b) IR monitor of the proton-coupled, CO binding reactivity.

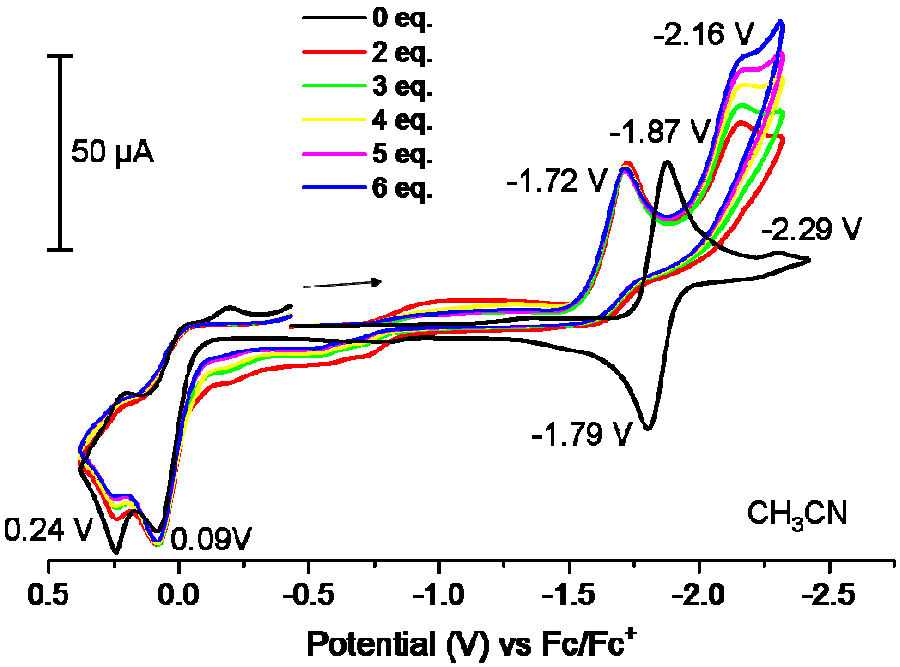

Figure S3. Cyclic voltammograms of complex **1** (2.5 mM) (black line) with AcOH (2, 3, 4, 5 and 6 equivalents) (colored lines) in 10 mL CH_3CN. All potentials are reported vs Fc^+/Fc (0.1 M [^{n}Bu$_4$N][PF$_6$] , scan rate = 50 mV/s, 22 °C).

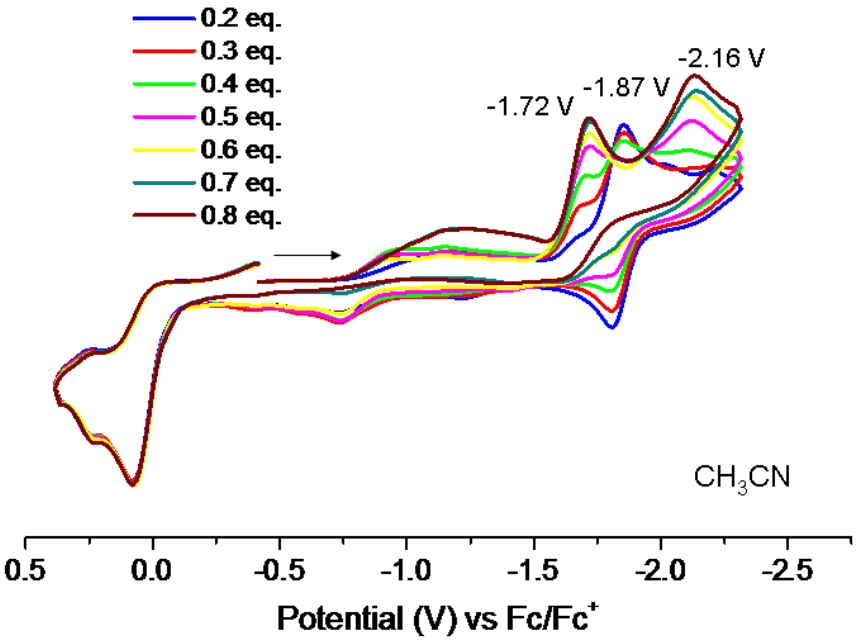

Figure S4. Cyclic voltammograms of complex **1** (2.5 mM) (black line) with AcOH (0.2, 0.3, 0.4, 0.5, 0.6, 0.7 and 0.8 equivalents) in 10 mL CH_3CN. All potentials are reported vs Fc^+/Fc (0.1 M [^{n}Bu$_4$N][PF$_6$] , scan rate = 50 mV/s, 22 °C).

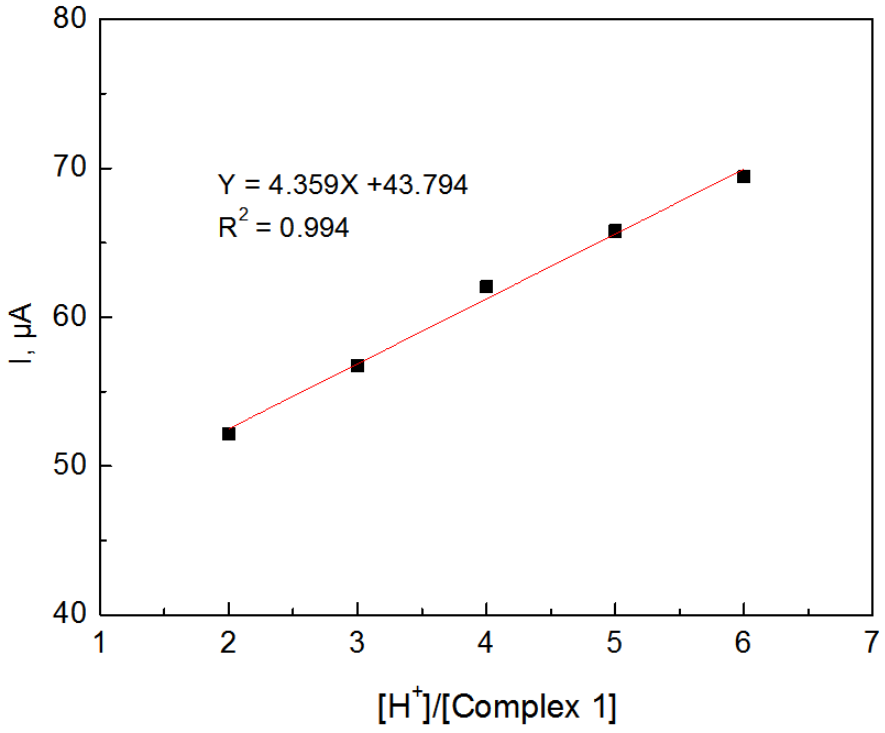

Figure S5. Dependence of current heights of electrocatalytic waves for complex **1** (2.5 mM) on acid concentration (5, 7.5, 10, 12.5, and 15 mM) in CH_3CN.

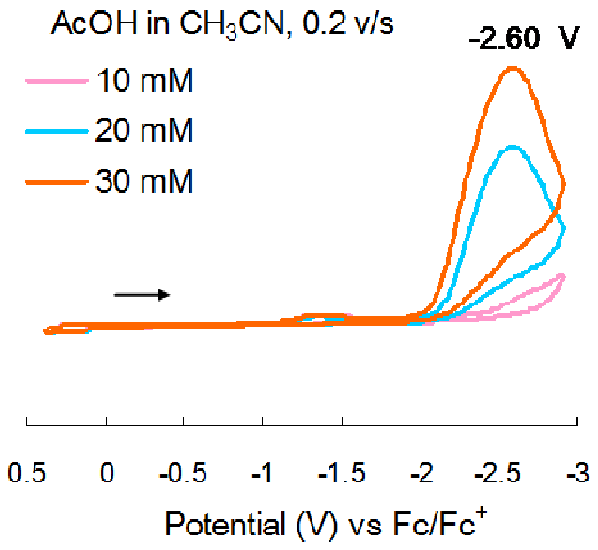

Figure S6. The cyclic voltammograms of AcOH (10, 20 and 30 mM) in MeCN.

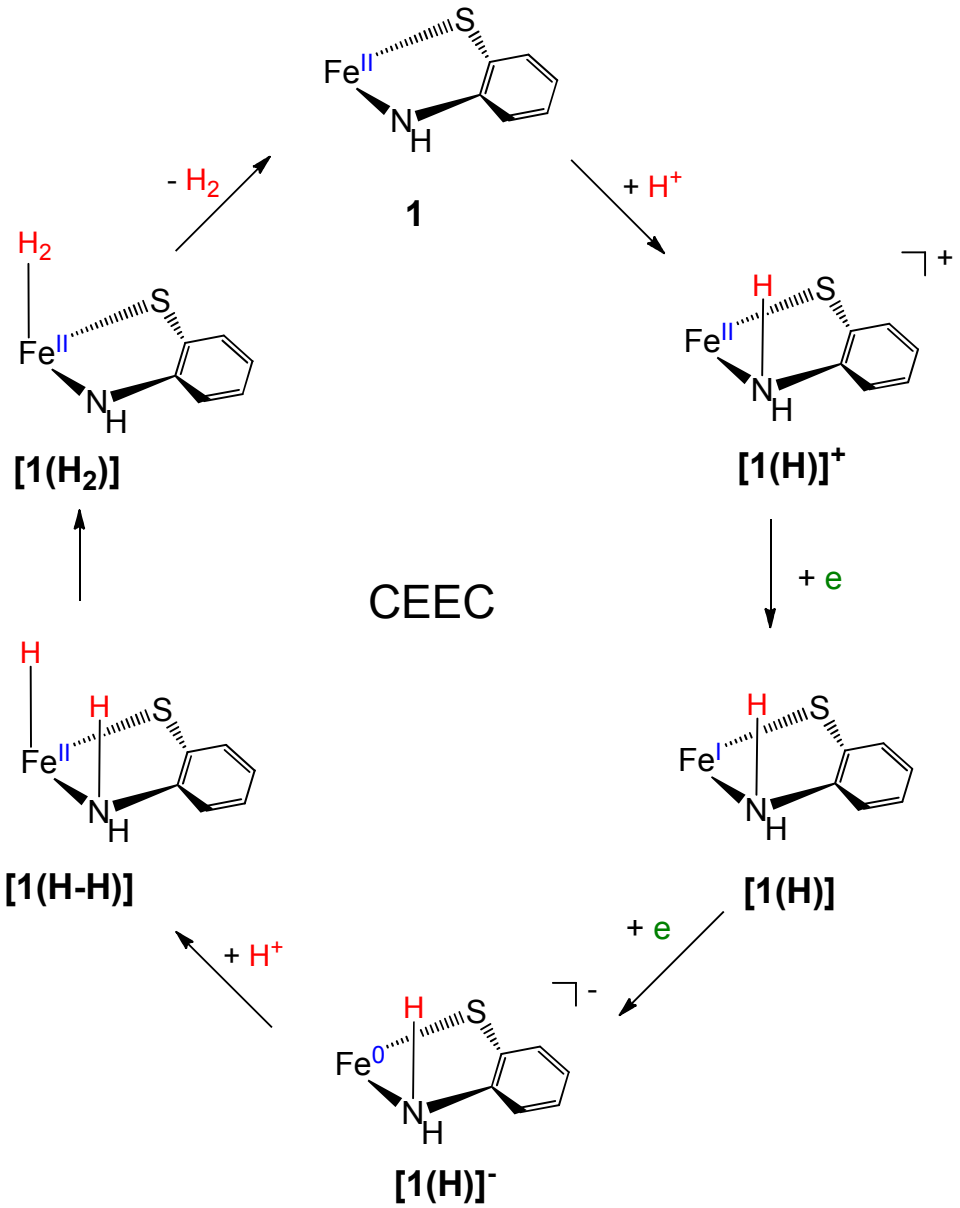

Figure S7. Proposed CEEC mechanism for H_2 produciton from AcOH reduction by complex **1** as electrochemical catalyst.

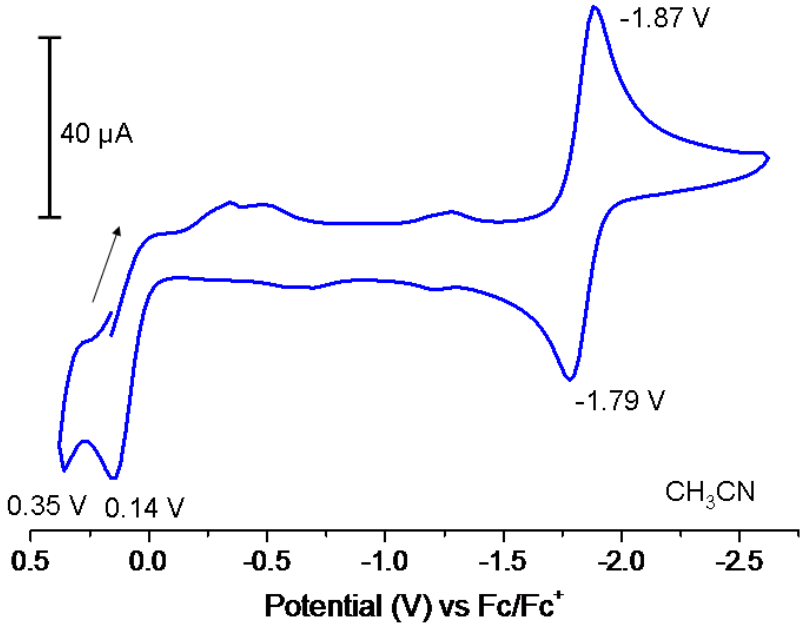

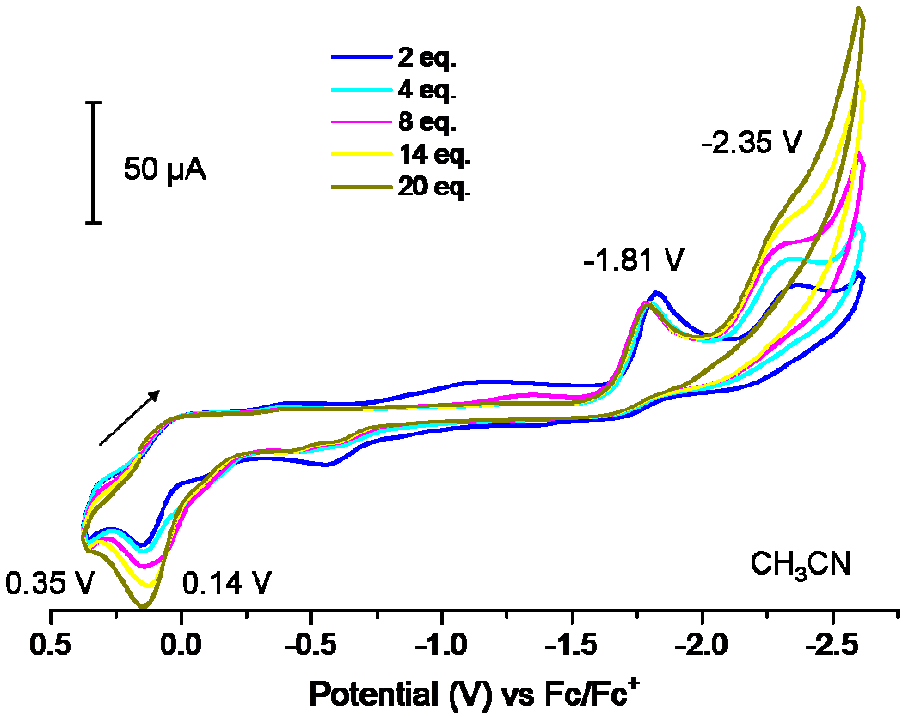

Figure S8. Cyclic voltammograms of complex **1** (2.5 mM) (Top) and complex **1** (2.5 mM) with added increments of AcOH (2, 4, 8,14 and 20 equivalents) (Bottom) in CH_3CN. All potentials are reported vs Fc^+/Fc (0.1M [^{n}Bu$_4$N][PF$_6$] , scan rate = 200 mV/s, 22 °C)

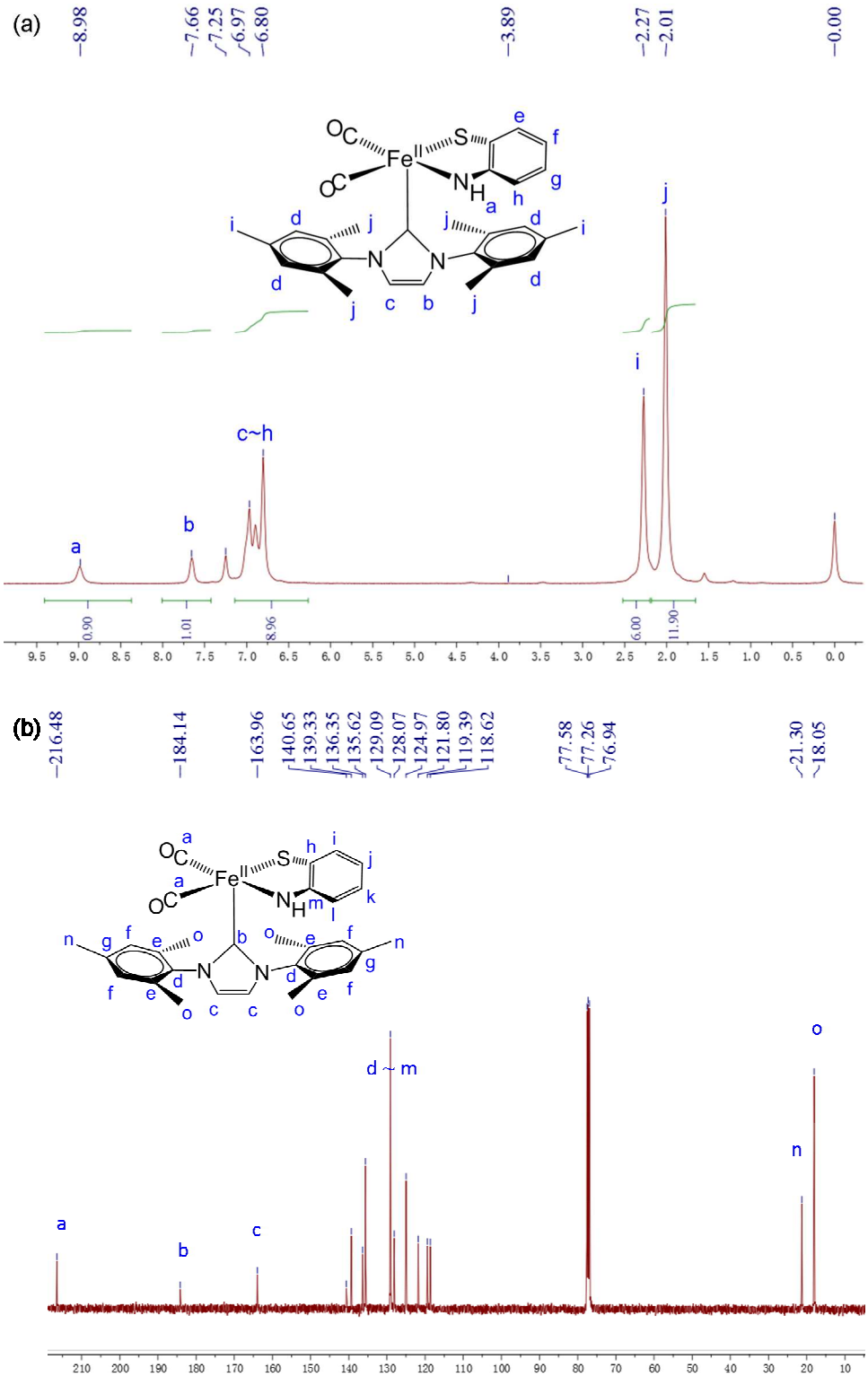

Figure S9. ^{1}H NMR (a) and ^{13}C NMR (b) spectra of complex **1**.

When τ = 0, the geometry is defined as square pyramid. When τ = 1, the geometry is defined as trigonal bipyramid. For the largest L-Fe-L' angles, the following is obtained.

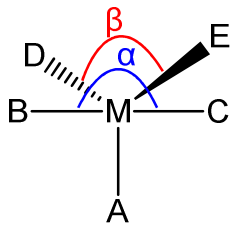

τ = (α-β)/60

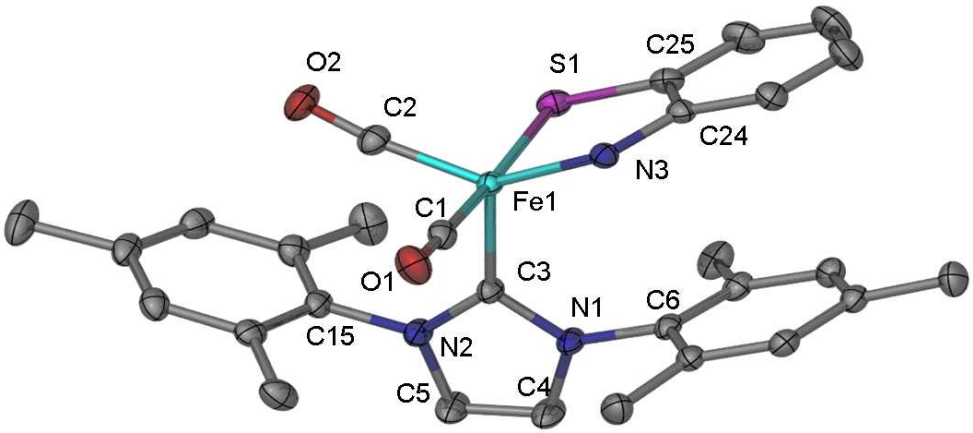

Complex **1**: $Fe(CO)_2IMes(NS)$

τ = (C1Fe1S1-C2Fe1N3)/60 = (172.12 - 141.77)/60 =0.506

Complex	τ
$Fe(CO)_2IMes(NS)$	0.506
$Fe(CO)_2PCy_3(NS)$	0.53[a]
$Fe(CO)_2PPh_3(NS)$	0.192[a]

[a] Ref.

(1) T. B. Liu, B. Li, C. V. Popescu, A. Bilko, L. M. Perez, M. B. Hall, M. Y. Darensbourg, *Chem-Eur J* **2010**, *16*, 3083.

Figure S10. Defining the geometry of complex **1**.

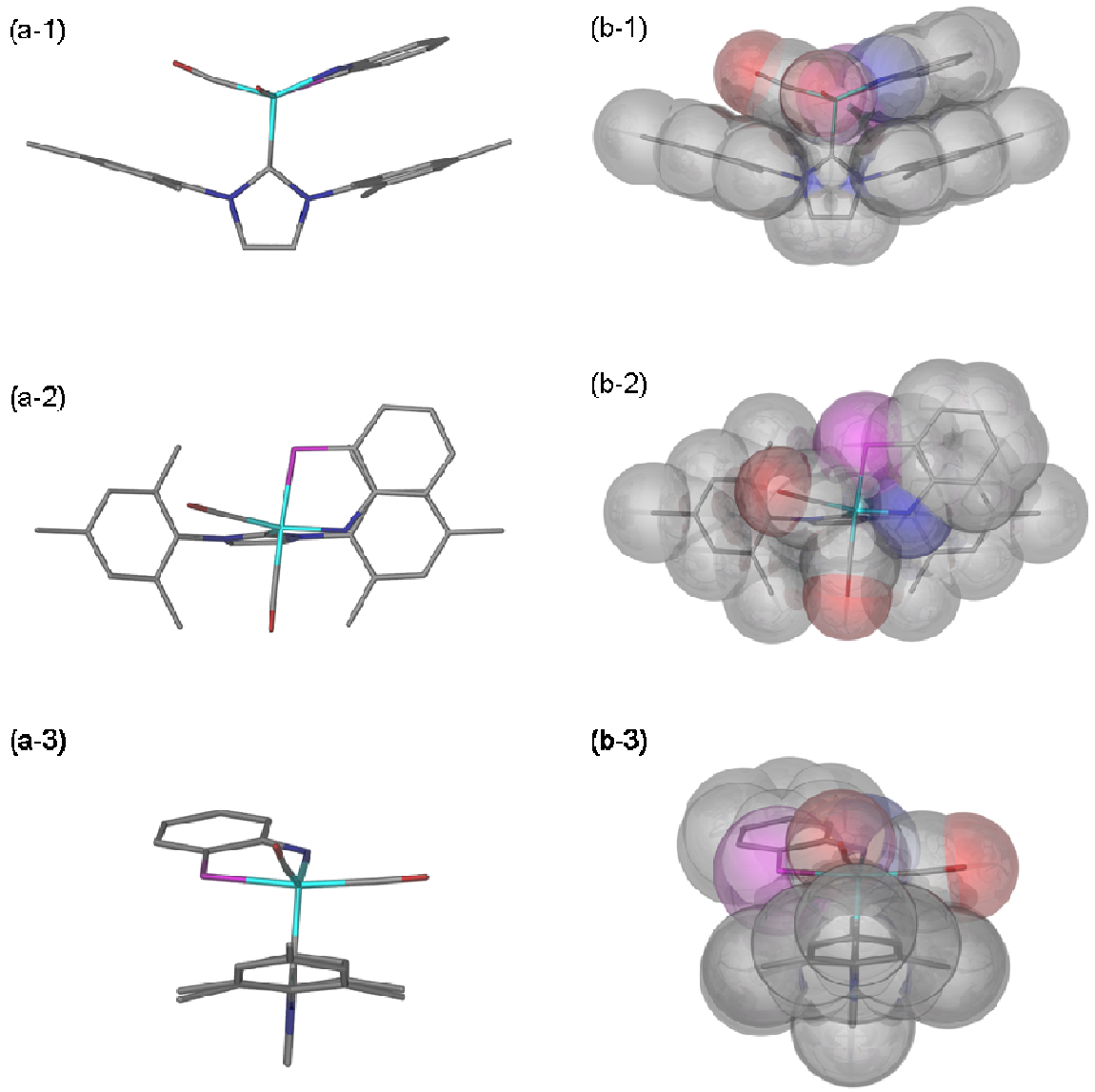

Figure S11. Stick drawing (a) and space-filling (b) models of complex **1** given in three perspectives.

Table S2. Crystallographic data and processing parameters for complex **1**

Complex	**1**
Empirical formula	$C_{29}H_{29}FeN_3O_2S$
Formula weight	539.46
Temperature	113(2) K
Wavelength	0.71075 A
Crystal system	Monoclinic
space group	P 21/n
a (Å)	10.2200(12)
b (Å)	19.200(2)
c (Å)	13.3650(17)
α (deg)	90
β (deg)	94.569(8)
γ (deg)	90
V (Å ^{3})	2614.2(5)
Z	4
*P*calcd (Mg/m^3)	1.371
Crystal size (mm^3)	0.24 × 0.22 × 0.20
$\theta_{min/max}$ (deg)	1.861/33.340
Reflections collected/unique	43635/10075
Parameters refined	335
GOF on F^2	1.112
$R1$ [$I > 2\ \sigma(I)$]	0.0427
$wR2$	0.1022
Residual electron density (e Å^{-3})	0.448, -0.534

Table S3. Selected bond length (Å) and angles (deg) for complex **1**

Fe(1)-C(2)	1.7676(14)
Fe(1)-C(1)	1.7755(14)
Fe(1)-N(3)	1.8545(11)
Fe(1)-C(3)	1.9535(12)
Fe(1)-S(1)	2.2330(5)
S(1)-C(25)	1.7213(14)
O(1)-C(1)	1.1456(17)
O(2)-C(2)	1.1456(17)
N(1)-C(3)	1.3626(16)
N(1)-C(4)	1.3827(17)
N(1)-C(6)	1.4356(16)
N(2)-C(3)	1.3559(16)
N(2)-C(5)	1.3870(17)
N(3)-C(24)	1.3675(16)
C(4)-C(5)	1.339(2)
C(24)-C(29)	1.4067(18)
C(24)-C(25)	1.4068(18)
C(25)-C(26)	1.401(2)
C(26)-C(27)	1.371(2)
C(27)-C(28)	1.399(2)
C(28)-C(29)	1.375(2)
C(2)-Fe(1)-C(1)	91.78(6)
C(2)-Fe(1)-N(3)	141.77(6)
C(1)-Fe(1)-N(3)	90.17(5)
C(2)-Fe(1)-C(3)	100.29(6)
C(1)-Fe(1)-C(3)	95.77(6)
N(3)-Fe(1)-C(3)	117.49(5)
C(2)-Fe(1)-S(1)	88.37(5)
C(1)-Fe(1)-S(1)	172.12(4)
N(3)-Fe(1)-S(1)	84.87(4)
C(3)-Fe(1)-S(1)	91.95(4)
C(25)-S(1)-Fe(1)	99.25(5)
C(24)-N(3)-Fe(1)	123.78(9)
O(1)-C(1)-Fe(1)	177.22(12)
O(2)-C(2)-Fe(1)	170.79(12)
N(2)-C(3)-N(1)	103.37(10)
N(2)-C(3)-Fe(1)	131.89(9)
N(1)-C(3)-Fe(1)	124.74(9)
C(26)-C(25)-S(1)	124.73(11)
C(24)-C(25)-S(1)	115.71(10)

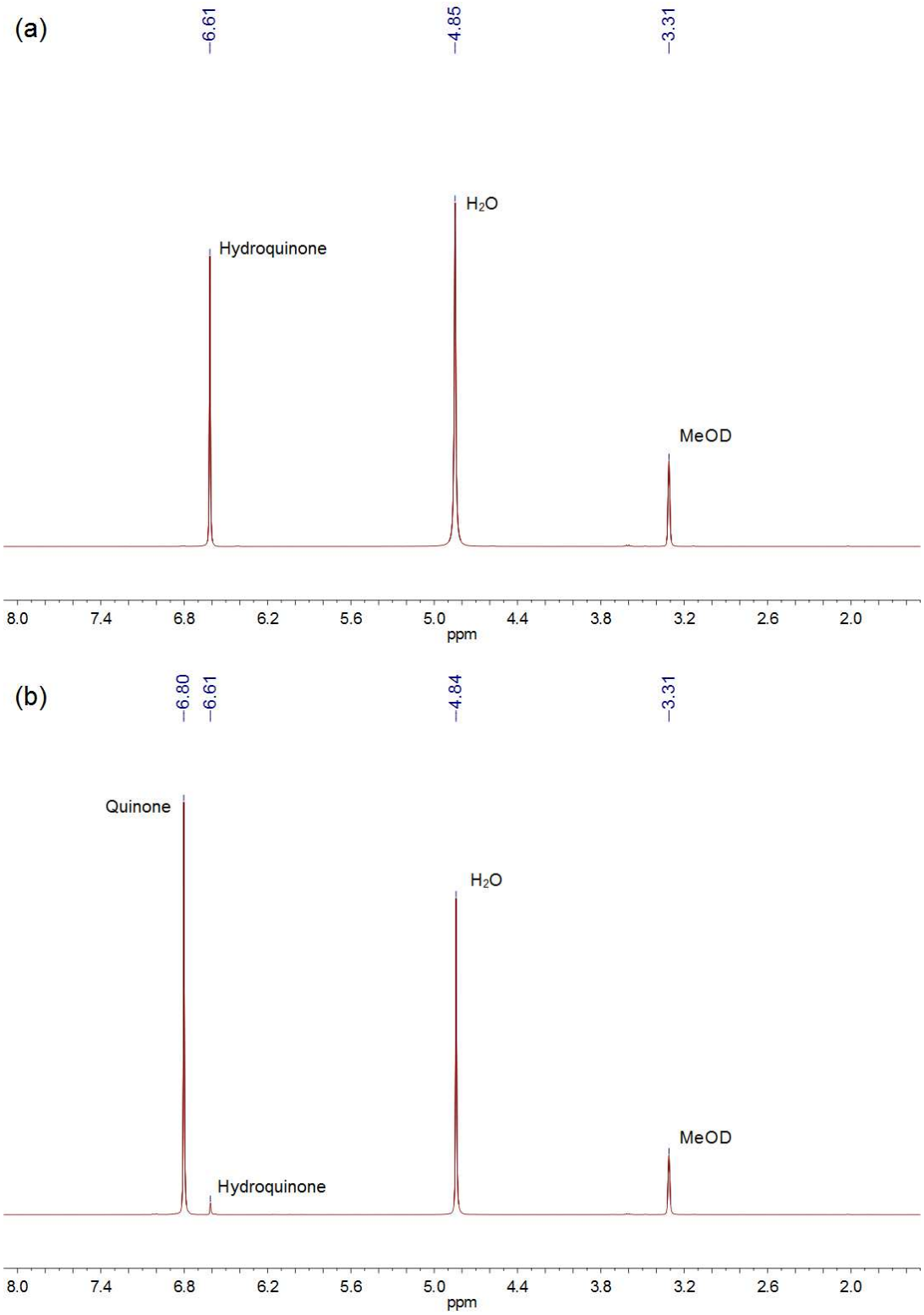

Figure S12. ^{1}H NMR spectrum of standard (a) hydroquinone and (b) quinone (with tiny amount of hydroquinone as impurity) in MeOD.

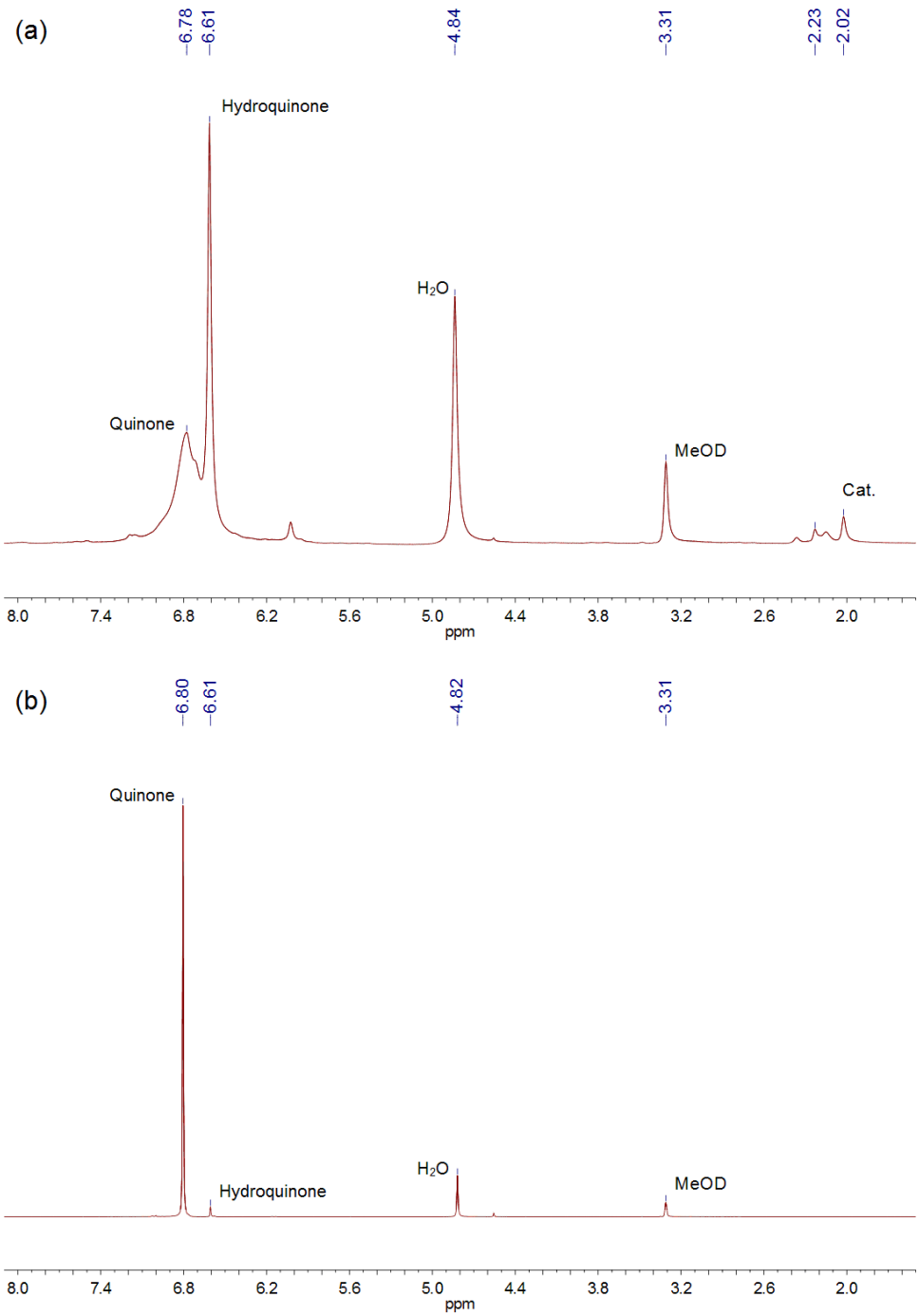

Figure S13. In-situ ^{1}H NMR spectrum monitor of the transfer hydrogenation of quinone to hydroquinone in MeOD at 25°C (a) with complex **1** as catalyst; (b) no complex **1** was added

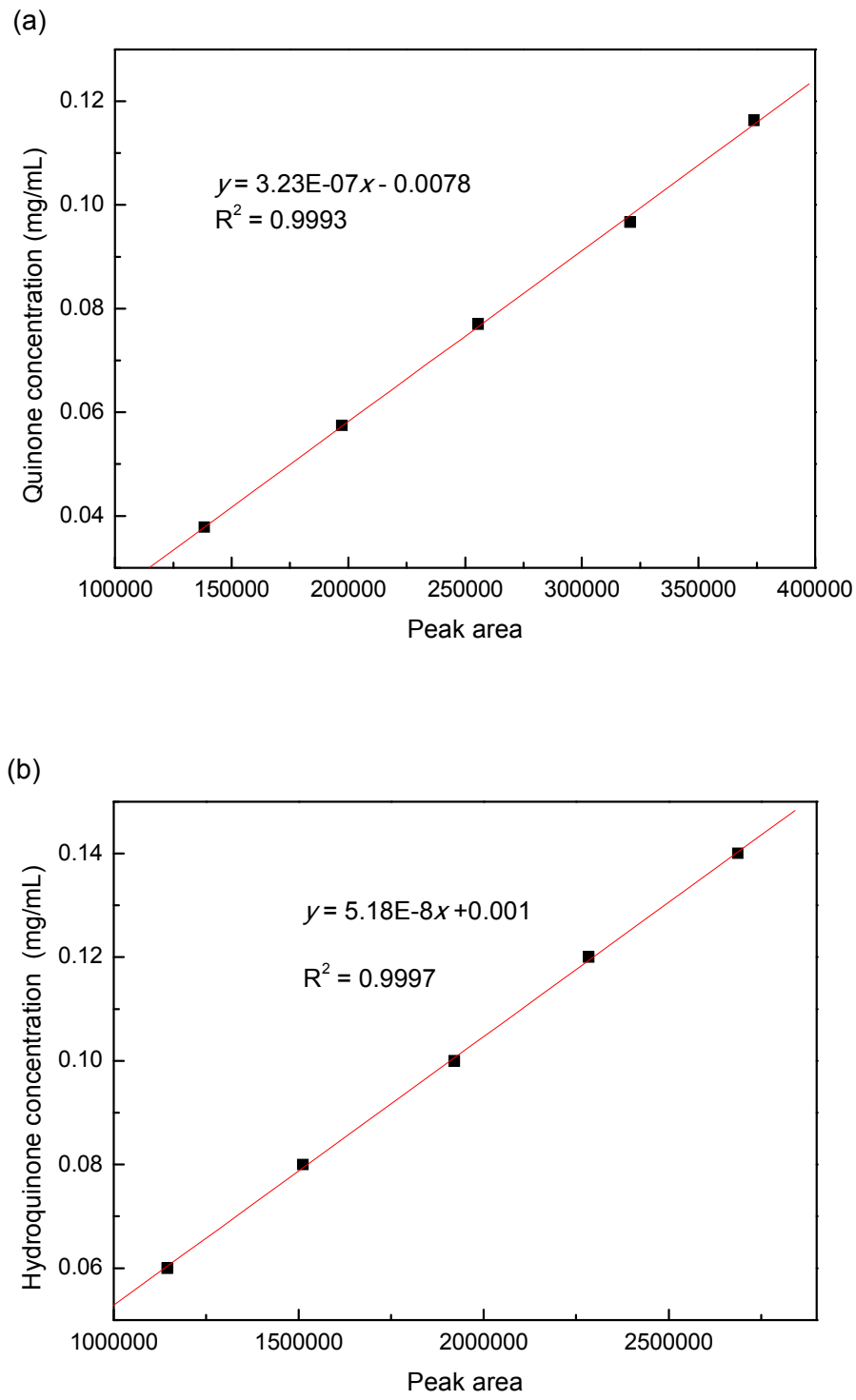

Figure S14. HPLC calibration curve of quinone (a) and hydroquinone (b).

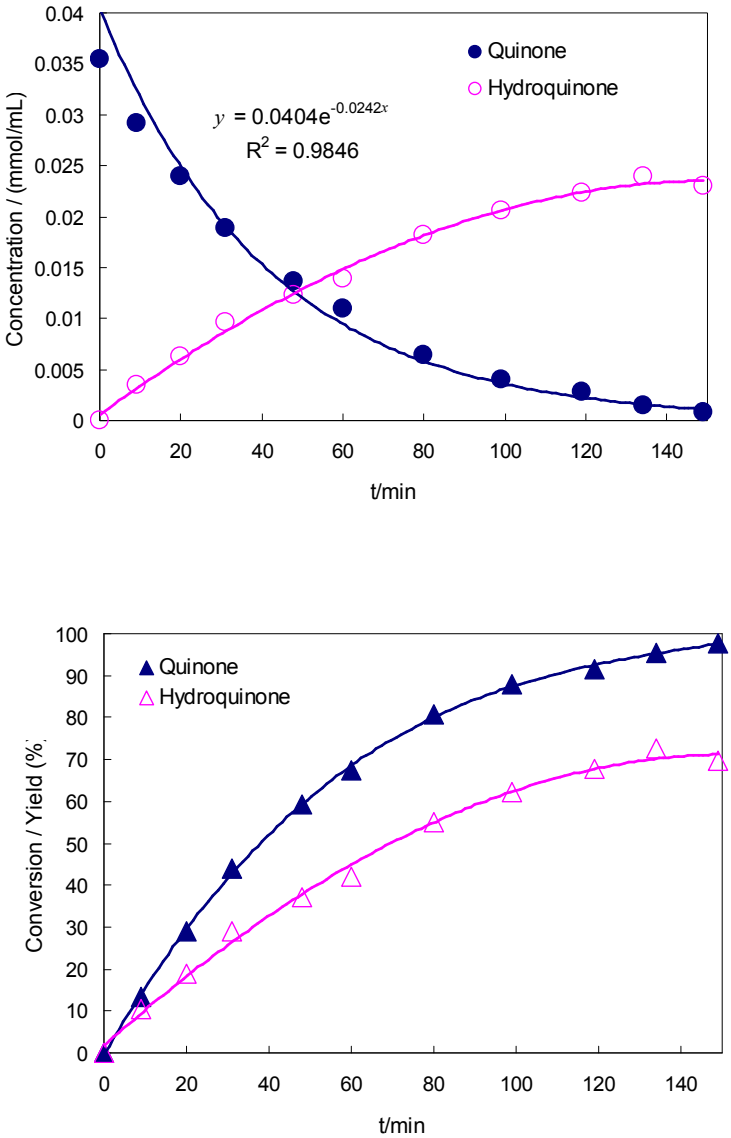

Figure S15. Top: Dependence of the concentration of quinone and hydroquinone on time at 40°C in methanol (1.2 mol% complex **1**). Bottom: Dependence of the conversion of quinone and the yield of hydroquinone on time at 40°C in methanol (1.2mol% complex **1**)

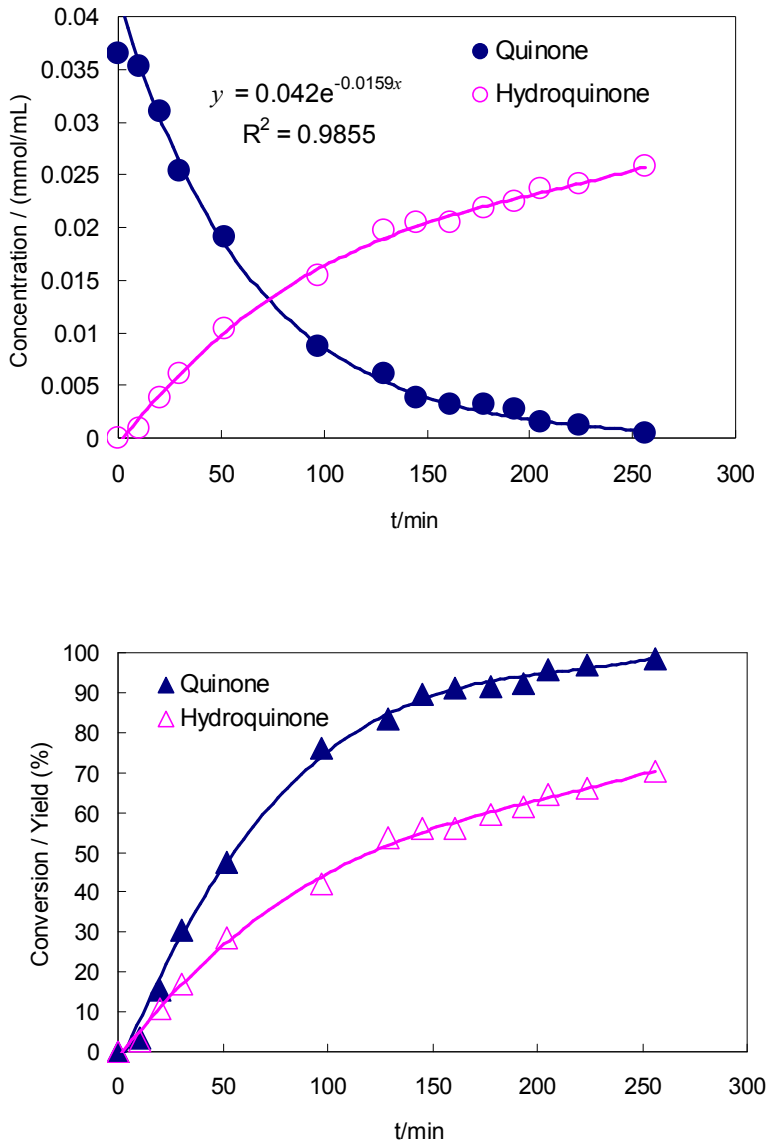

Figure S16. Top: Dependence of the concentration of quinone and hydroquinone on time at 35°C in methanol (1.2 mol% complex **1**). Bottom: Dependence of the conversion of quinone and the yield of hydroquinone on time at 35°C in methanol (1.2 mol% complex **1**)

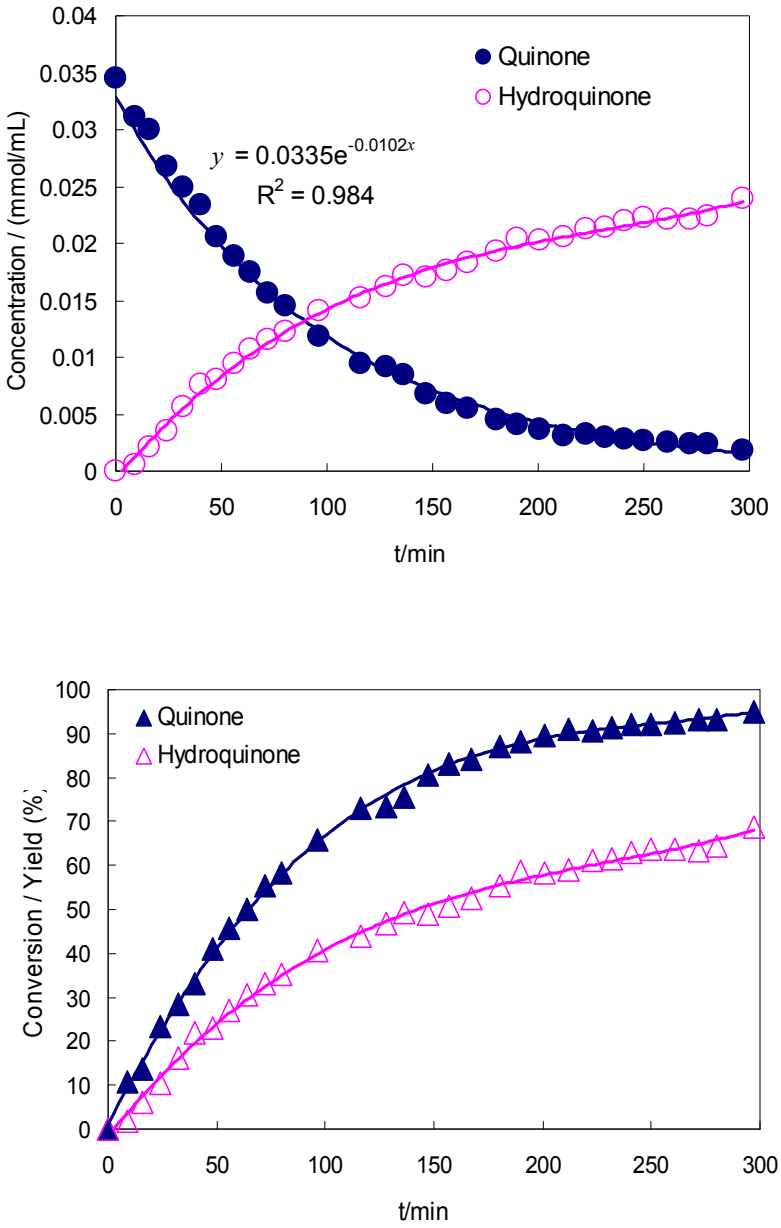

Figure S17. Top: Dependence of the concentration of quinone and hydroquinone on time at 30°C in methanol (1.2 mol% complex **1**). Bottom: Dependence of the conversion of quinone and the yield of hydroquinone on time at 30°C in methanol (1.2 mol% complex **1**)

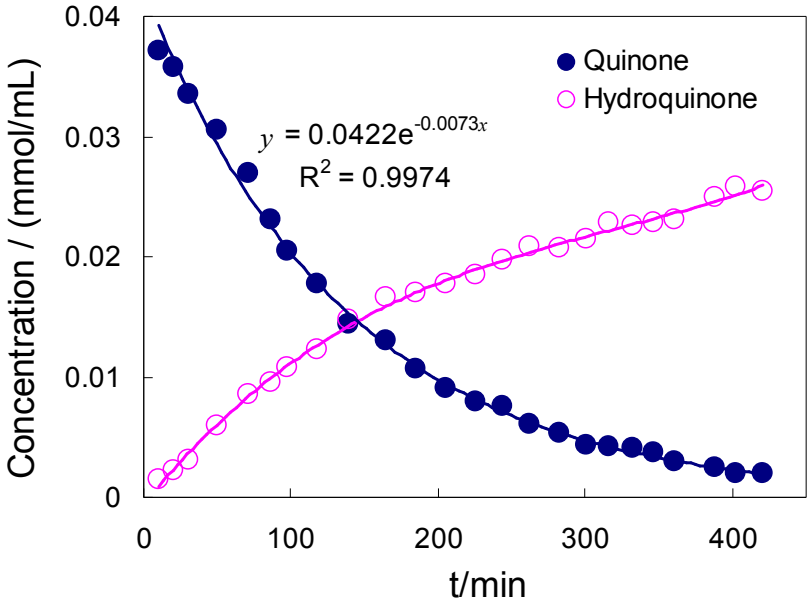

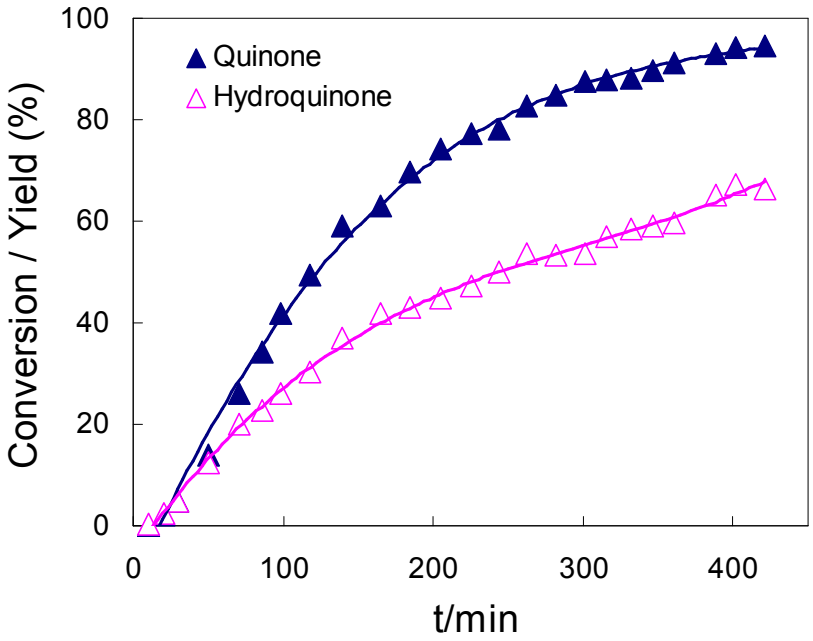

Figure S18. Top: Dependence of the concentration of quinone and hydroquinone on time at 25°C in methanol (1.2 mol% complex **1**). Bottom: Dependence of the conversion of quinone and the yield of hydroquinone on time at 25°C in methanol (1.2 mol% complex **1**)

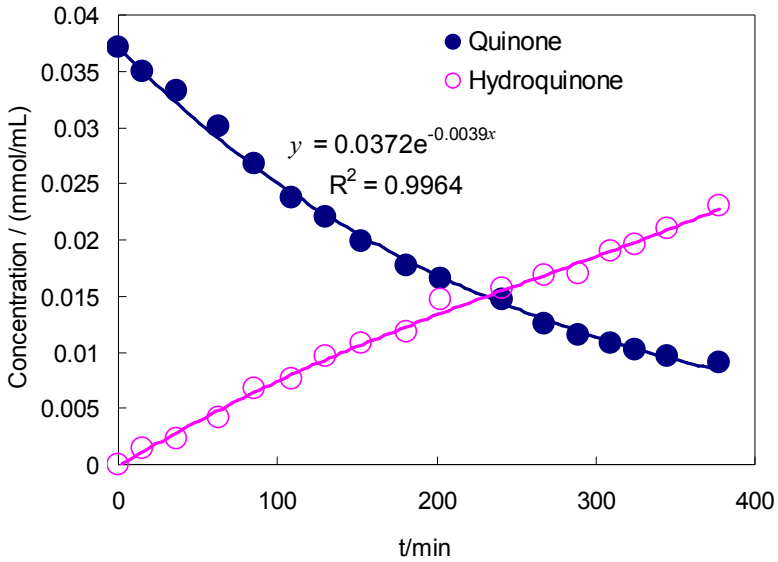

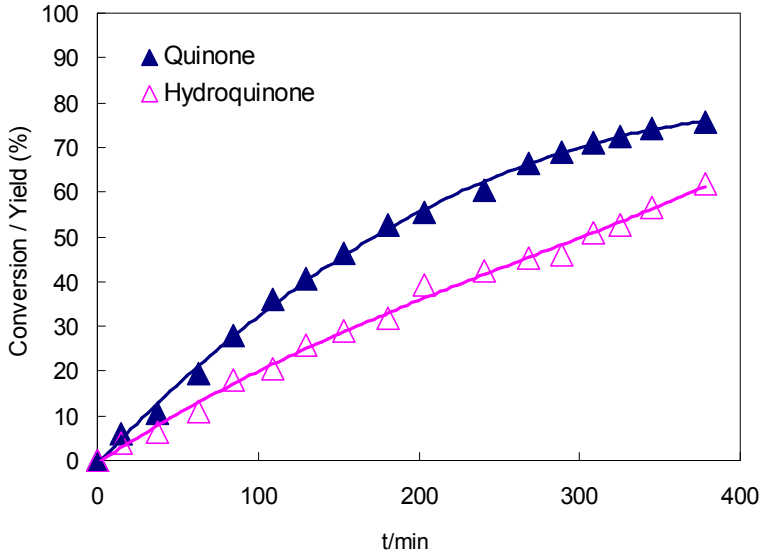

Figure S19. Top: Dependence of the concentration of quinone and hydroquinone on time at 20°C in methanol (1.2 mol% complex **1**). Bottom: Dependence of the conversion of quinone and the yield of hydroquinone on time at 20°C in methanol (1.2 mol% complex **1**)

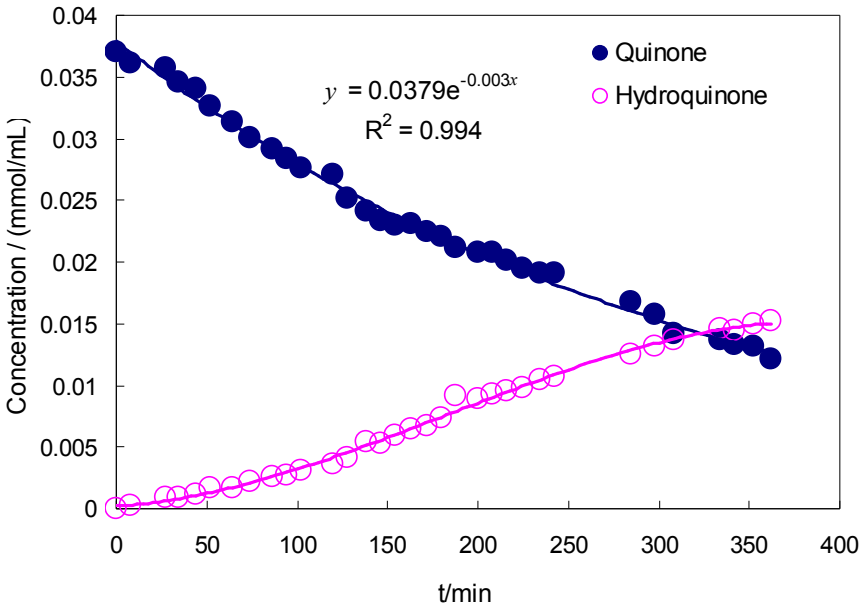

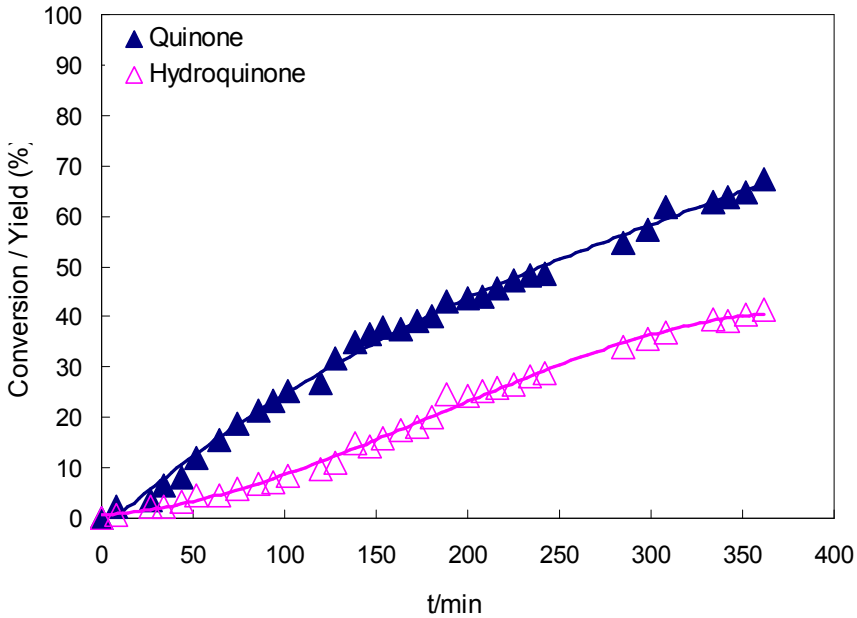

Figure S20. Top: Dependence of the concentration of quinone and hydroquinone on time at 15°C in methanol (1.2 mol% complex **1**). Bottom: Dependence of the conversion of quinone and the yield of hydroquinone on time at 15°C in methanol (1.2 mol% complex **1**)

Control experiment: The monitor of concentration of quinone without addition of complex **1** at 25°C. (Especially the detection of hydroquinone at the start of this reaction was due to the existence of hydroquinone as impurity in quinone starting material.)

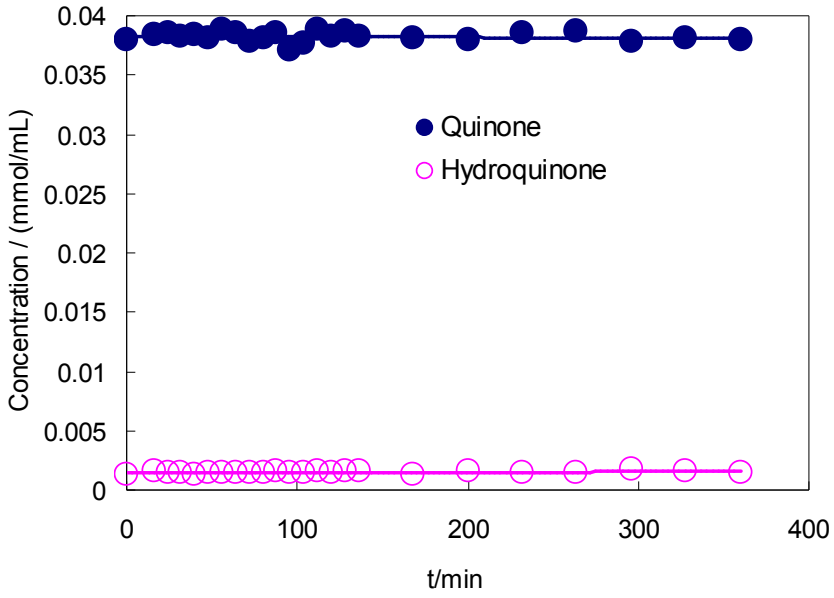

Figure S21. Dependence of the concentration of quinone and hydroquinone on time at 25°C in methanol (no complex **1**).

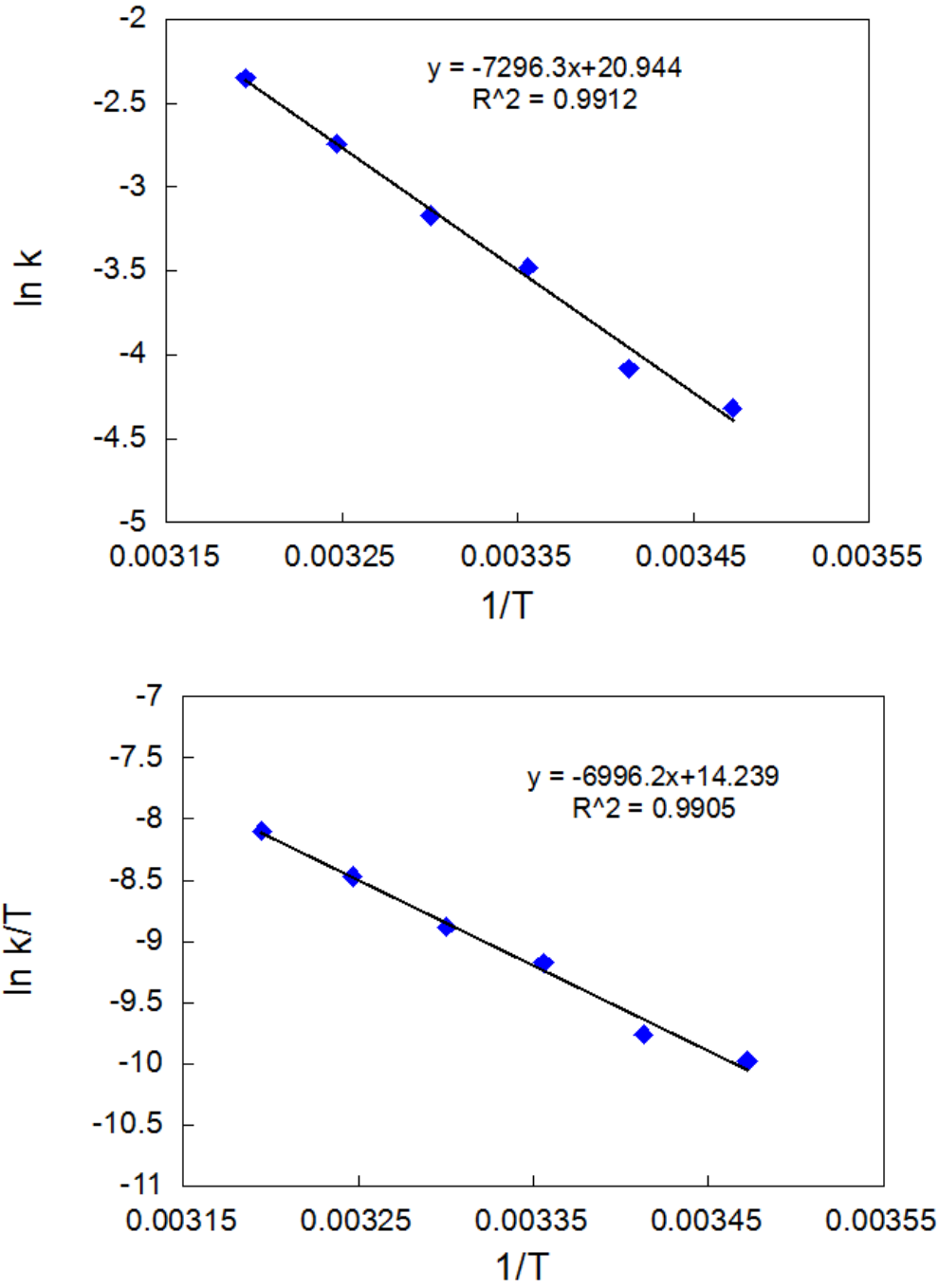

Figure S22. Top: Arrhenius plots for the transfer hydrogenation process of quinone. Bottom: Eyring plot for the hydrogenation process of quinone (1.2 mol% complex **1**).

Table S4. Temperature dependence of transfer hydrogenation of quinone.

T (K)	10^4 k_{obs} (s^{-1})	Activation parameters [a]
288	0.50	*E*a = 64.3 kJ/mol
293	0.65	$\Delta H^{\ddagger}$ = 61.8(±2.3) kJ/mol
298	1.21	$\Delta S^{\ddagger}$ = -113.1(±7.5) J/mol K
303	1.70	
308	2.67	
313	4.03	

[a] Errors in activation parameters reported at 95% confidence level.